Chem Soc Rev

REVIEW ARTICLE

View Article Online
View Journal | View Issue

Cite this: *Chem. Soc. Rev.*, 2014, 43, 3426

Nanomaterials enhanced surface plasmon resonance for biological and chemical sensing applications

Shuwen Zeng,[a] Dominique Baillargeat,[c] Ho-Pui Ho[d] and Ken-Tye Yong*[ab]

The main challenge for all electrical, mechanical and optical sensors is to detect low molecular weight (less than 400 Da) chemical and biological analytes under extremely dilute conditions. Surface plasmon resonance sensors are the most commonly used optical sensors due to their unique ability for real-time monitoring the molecular binding events. However, their sensitivities are insufficient to detect trace amounts of small molecular weight molecules such as cancer biomarkers, hormones, antibiotics, insecticides, and explosive materials which are respectively important for early-stage disease diagnosis, food quality control, environmental monitoring, and homeland security protection. With the rapid development of nanotechnology in the past few years, nanomaterials-enhanced surface plasmon resonance sensors have been developed and used as effective tools to sense hard-to-detect molecules within the concentration range between pmol and amol. In this review article, we reviewed and discussed the latest trend and challenges in engineering and applications of nanomaterials-enhanced surface plasmon resonance sensors (*e.g.*, metallic nanoparticles, magnetic nanoparticles, carbon-based nanomaterials, latex nanoparticles and liposome nanoparticles) for detecting "hard-to-identify" biological and chemical analytes. Such information will be viable in terms of providing a useful platform for designing future ultrasensitive plasmonic nanosensors.

Received 29th December 2013

DOI: 10.1039/c3cs60479a

www.rsc.org/csr

1. Introduction and background

Surface plasmon resonance (SPR) sensors are powerful tools for real-time monitoring interactions of various biological and chemical analytes.[1–5] Their unique abilities for characterizing and quantifying low molecular weight molecules have led to their wide applications in theranostics, pharmaceutics, food safety, environmental monitoring and homeland security.[6,7] SPR sensors are optical refractometers that can measure refractive-index changes of the medium at the SPR sensing surfaces. The working principle of SPR sensors is based on a unique and simple optical phenomenon. In this phenomenon, the collective coherent oscillations of free electrons in the conduction band of a metal is first excited by the interactive electromagnetic field at a metal/dielectric interface[8–10] and these created charge density oscillations are called surface plasmon polaritons (SPPs). The SPPs will then form an electric field that exponentially decays into its surrounding medium with a penetration depth in hundreds of nanometers range. As a result, this evanescent field is highly sensitive towards the refractive-index change of the surrounding medium. Thus, when the refractive index of the sensing medium changes the characteristics (*e.g.*, angle, wavelength, phase, *etc.*) of the incident light beam for SPR excitation will change accordingly.

There are two main types of SPR sensors: propagating SPR (PSPR) sensors and localized SPR (LSPR) sensors.[11] PSPR is usually excited on continuous metal thin films through prism couplers or grating and PSP resonance can propagate along the metal/dielectric surface up to hundreds of micrometers,[12] while LSPR is nonpropagating surface plasmon excited on nanostructured metal surfaces and LSP resonance can be tuned by their size, shape and composition.[13] Although LSPR sensors have much better spectral tunabilities, their sensitivities are orders of magnitude lower than those of PSPR sensors.[14,15] In addition, it is difficult for both PSPR and LSPR sensors to directly detect analytes at extremely dilute concentration (less than 1 pM) or with small molecular weight (less than 8 kDa).[14,16,17] To overcome this challenge of SPR sensors, many sensitivity-enhancement methods have been proposed and reported as shown in Scheme 1, most of which are based on nanomaterials including metallic

[a] *School of Electrical and Electronic Engineering, Nanyang Technological University, Singapore, 639798, Singapore. E-mail: ktyong@ntu.edu.sg*
[b] *Novitas, Nanoelectronics Centre Of Excellence, Nanyang Technological University, 50 Nanyang Avenue, Singapore 639798, Singapore*
[c] *CINTRA CNRS/NTU/THALES, UMI 3288, Research Techno Plaza, 50 Nanyang Drive, Border X Block, Singapore, 637553, Singapore*
[d] *Department of Electronic Engineering, The Chinese University of Hong Kong, Hong Kong*

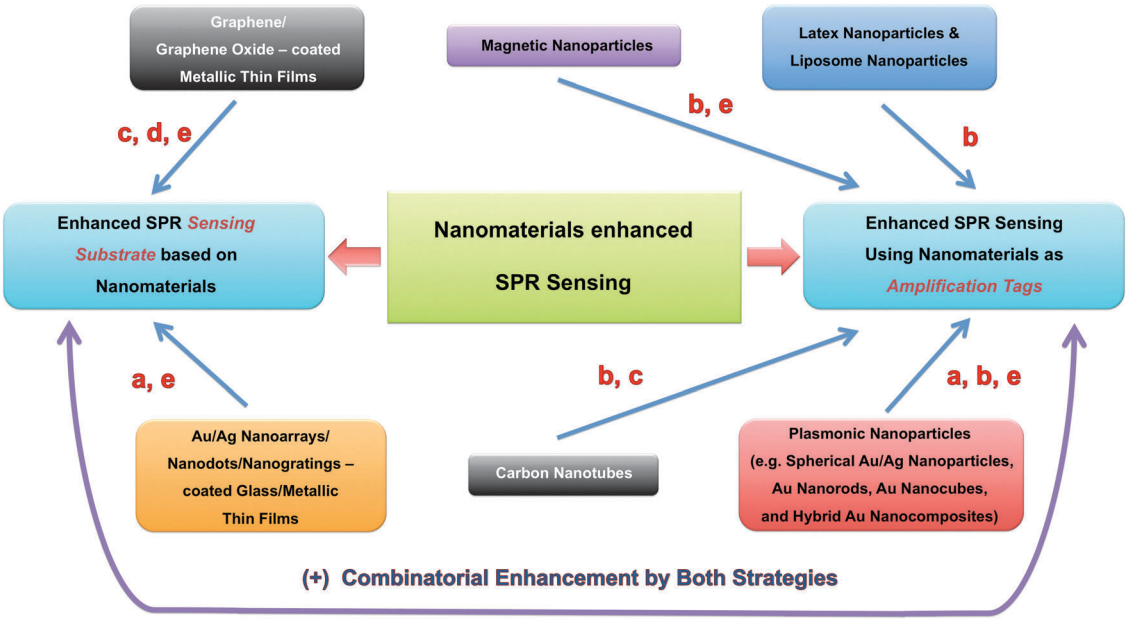

Scheme 1 Various types of nanomaterials for enhanced SPR sensing. Enhanced mechanisms: (a) electric field enhancement by coupling the LSPR excited on the surface of nanomaterials with the surface plasmon wave (SPW) excited on the sensing film; (b) large surface mass loading of the nanomaterials leading to large perturbations on the sensing surface; (c) charge transfer from the nanomaterial surface to the metallic sensing film surface that would induce larger evanescent field enhancement thereby magnifying the SPR signals; (d) enhanced adsorption efficiency due to pi-stacking force between target analyte and the nanomaterial surface; (e) catalytic activity of functionalized nanomaterials to further trigger secondary signal amplification – optional.

nanoparticles (*e.g.*, Au and Ag nanoparticles), magnetic nanoparticles, carbon-based nanostructures (*e.g.*, graphene), latex nanoparticles and liposome nanoparticles.[12,13,18–21] This scheme will serve as a useful platform for the researchers to have a bird's-eye view of the current state-of-art of using various nanomaterials for enhanced SPR sensing applications ranging from medicine to environmental monitoring. More importantly, this scheme will allow one to select the most appropriate enhanced mechanisms for engineering the specific type of nanomaterial-based enhanced SPR sensing system for detecting the desired biological or chemical molecules in different solvents. It is worth noting that the two main strategies as introduced in Scheme 1, (i) enhanced SPR sensing substrate based on nanomaterials and (ii) enhanced SPR sensing using nanomaterials as amplification tags can be further combined to achieve a greater SPR sensing performance.

Noble metallic nanoparticles, especially gold nanoparticles (Au NPs), are commonly used nanomaterials for improving the sensing performance of PSPR sensors.[12,14,16] These particles are also called plasmonic nanoparticles. They exhibit strong absorption in the visible and near-infrared wavelength regions. Consequently, a large electric field due to LSPR will be excited on the surface of the particles. It has been demonstrated that the SPR sensitivity is closely related to the excited electric field: the larger the electric field, the more sensitive of SPR sensors to the change of its surrounding medium.[16] Coupling the LSPR with surface plasmon waves generated from metal thin film on a conventional PSPR sensor is found to be an efficient way to obtain a larger field enhancement thereby resulting in a higher sensitivity. Also, the ease of functionalizing the metallic nanoparticle's surface with various functional molecules allows one to tailor the surface coverage and binding efficiency of target molecules on the surface of the particle for specifically interacting with the sensing film.[13] Recently, functionalized magnetic nanoparticles (MNPs) such as Fe_3O_4 nanoparticles have been employed for signal amplification of PSPR sensors as well.[18,22–25] Compared to plasmonic nanoparticles, the main advantages of using MNPs are that the production cost of the MNPs is lower and the step for initial receptor immobilization onto the SPR sensing film is not needed.[18] Moreover, the MNPs can be attracted and manipulated by externally applied magnetic fields and form an "aggregate" layer with a strong refractive index contrast on the metallic sensing film that will lead to a notable SPR signal when sensing trace amounts of biological and chemical samples.[18,22] Besides having such improved sensitivities, these nanoparticle-enhanced PSPR sensors also retain the advantages of conventional PSPR sensors such as flexibility in quantitative and kinetic analyses of biomolecules that are a challenging to perform using the complementary counterpart of the optical sensing tools such as fluorescence sensors.[26–28]

In addition to the above-mentioned zero/one-dimensional nanoparticles as SPR signal amplification tags, two-dimensional nanostructures have recently been developed and integrated into the SPR sensing films for both sensitivity enhancement and preserving the label-free feature of the SPR sensors.[14,29–31] For example, Kabashin *et al.*[14] designed a novel SPR sensing film consisting of Au nanorod metamaterials, which can be used to support the guided mode in the nanorod layer and achieved a detection limit of 10 μM for biotin with a small molecular weight of 244 Da (Fig. 1). The interactions between the targeted biological substances and the functionalized nanorods are within the

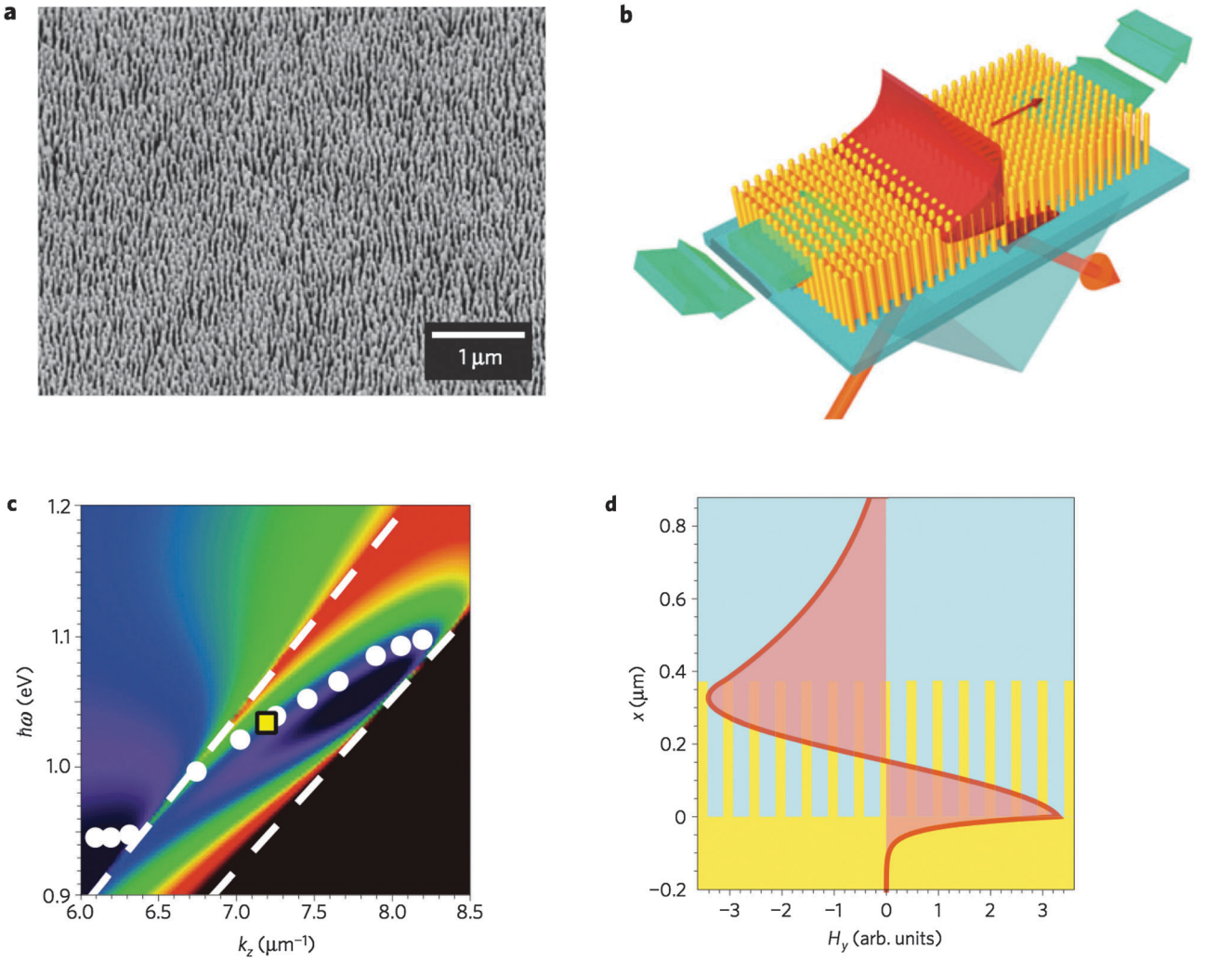

Fig. 1 Plasmonic nanorod metamaterial and the properties of the electromagnetic mode used for enhanced SPR sensing experiments. (a) Typical scanning electron micrograph of the nanorod assembly. (b) Schematic of the ATR measurements and flow cell. (c) Dispersion of the guided mode in the metamaterial–water system. Colour plot: numerical simulations; circles: experimental dispersion plotted from (b); dashed lines: light lines in air (top left) and the substrate (bottom right). (d) The calculated electromagnetic-field distribution of the guided mode in the metamaterial layer. The profile corresponds to the position indicated by the yellow square in (c). Reproduced from ref. 14 with permission of Nature Publishing Group.

strong probing field that arises from the substantial overlap of excited electric field of the LSPR of Au nanorods inside the sensing layer. Recently, graphene-modified SPR sensing substrates have attracted much attention from the scientific community.[19,31–36] It has been demonstrated that coating graphene layers on gold or silver thin films can induce larger SPR signal changes compared to those with bare metal thin films.[19,34] This is mainly due to the charge transfer from graphene to the surface of metal thin film since their work function is different and this effect has led to a strong excited electric field enhancement at the sensing surface.[37] Also, the highly selective adsorption of aromatic rings structure molecules (*e.g.*, DNA and TNT) on the surface of graphene-modified SPR sensing substrate can be achieved through strong pi-stacking forces and this specific interaction will certainly open new avenues for ultra-sensitive detections of peptides, DNA, RNA and siRNA molecules.[19,38]

In this review, we discuss the current state-of-the-art developments and challenges of employing nanomaterials-enhanced surface plasmon resonance sensors for detecting chemical and biological analytes ranging from nucleic acids to hormones and from harmful chemicals to explosive materials. We first discuss the different types of gold nanoparticles-enhanced SPR sensors available in the literature and markets and subsequently we highlight their individual unique capabilities for detecting biological and chemical substances in Section 2, following by a detailed review in Section 3 on designing new types of enhanced SPR sensors based on other novel nanomaterials such as magnetic nanoparticles, carbon-based nanomaterials, silver nanoparticles, latex nanoparticles and liposome nanoparticles. Finally, Section 4 highlights the summary and future outlook for engineering the nanomaterials to further improve plasmonic sensing of hard-to-detect small molecules.

This review article is intended to promote the awareness of current developments of nanomaterials-based SPR sensors in biological and chemical sciences, the potential applications of

nanomaterials-based SPR sensors in environmental sensing and monitoring, and the approaches to optimize their sensitivity with the incorporation of nanomaterials. It succinctly discusses key *in vitro* sensing studies in various biological samples. This discussion will encourage the nanomaterials community to think about possible clinical applications of nanomaterials-based SPR sensors such as early cancer diagnosis, food quality control and drug screening.

2. Gold nanoparticles-amplified SPR sensors

Gold nanoparticles have been commonly used as signal-amplification labels in conventional PSPR sensors.[39–41] The LSPR peaks of gold nanoparticles are strongly governed by their size, shape and the dielectric constant of the surrounding medium. For example, the LSPR of gold nanorods (Au NRs) can be systematically tuned from the visible to the near-infrared wavelength region by carefully manipulating their aspect ratios.[42,43] Thus, one can pick the ''right'' gold particle size and couple its corresponding LSPR to the surface plasmon waves of PSPR sensors for obtaining the largest field enhancement effect thereby increasing the sensitivity of the sensor. For instance, our group has discovered that the size of Au NPs played an important role in manipulating the enhancement of surface plasmon resonance (SPR) sensing signals.[12] We have simulated the perturbation of the evanescent field in the presence of Au NPs of different sizes (Fig. 2). The results have shown that Au NPs with 40 nm possess the highest coupling effect when the separation of Au NP and SPR sensing films is fixed at 5 nm. Our experimental results show good agreement with the theoretical study. In addition, Golden *et al.*[44] reported the examination of the impact of the coupling distance (0–26 nm) between Au NP and the SPR sensing film and the SPR excitation wavelength (540 nm to 780 nm) on the dielectric function of Au NPs when

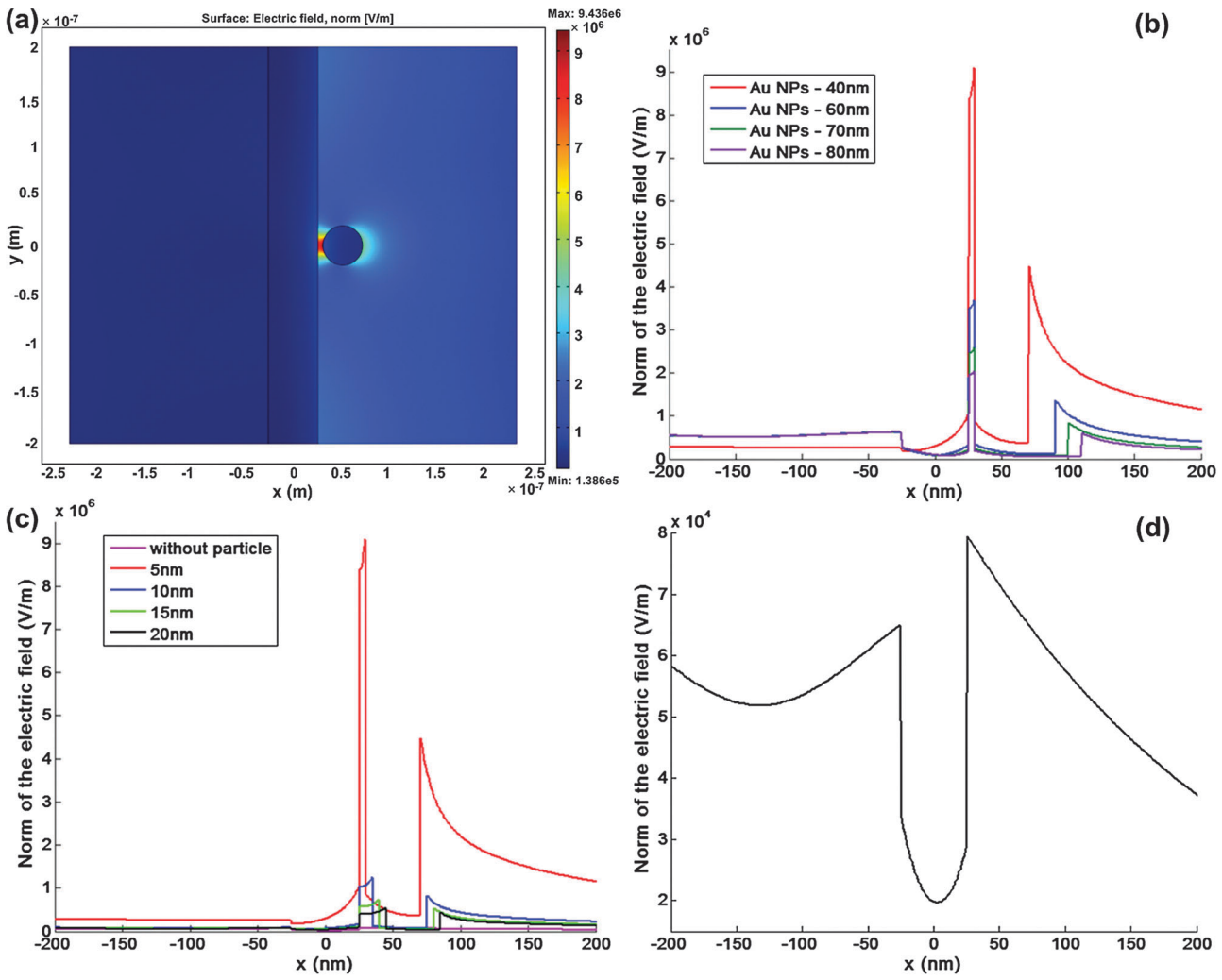

Fig. 2 Finite element analysis (FEA) simulations of resonant spherical-Au NPs coupling to the sensing film: (a) normal of the electric field with Au NPs (diameter is 40 nm, distance from the film is 5 nm), cross-section plots for the electric field along $y = 0$, (b) Au NP with different diameters, (c) different distances between Au NP (40 nm in diameter) and the Au film, (d) without Au NP. The electric fields for Au NP with diameter in 60 nm, 70 nm and 80 nm in (b) are magnified by a factor of 10 for clarity. Reproduced from ref. 12 with permission of Elsevier.

the diameter of Au NP was fixed at 10 nm. They have calculated the intrinsic dielectric constants of Au NPs by fitting the measured SPR reflectance curves through a modified Maxwell–Garnett model. It was found that when the coupling distance was smaller than 10 nm, the intrinsic dielectric function of Au NP had a large variation in values and showed an anomalous dispersion behavior. Basically, the real part of the Au NP dielectric constant (ε_r) was varied from −12 to −2 along with the SPR excitation wavelength varying from 540 nm to 780 nm and it was observed that the imaginary part of the Au NP dielectric constant (ε_i) increases significantly as excitation wavelength (λ_{exc}) increases. Whereas when the coupling distance was larger than 10 nm, the intrinsic dielectric function of Au NP displayed a normal dispersion and it was found that ε_r decreased with increasing λ_{exc} and ε_i was discovered to be independent of the coupling distance for all of the studied λ_{exc}. Thus, all these studies indicate that by carefully designing the size and shape of Au NPs as well as the particle coupling distance to sensing film, one can obtain an optimal set of experimental sensing parameters to detect interested biomolecules under extremely low concentration conditions. The preparation of gold nanoparticles with different sizes and shapes are relatively simple and straightforward by following the synthesis recipes reported in the literature.[45,46] For example, colloidal spherical Au NPs with diameters of 15–150 nm can be prepared using the well-known Turkevitch method where Au particles are formed by reducing $HAuCl_4$ with sodium citrate in boiling water.[47–49] As for Au NRs, different aspect ratios of particles can be synthesized by employing the seed-mediated growth method and the detailed synthesis protocols can be obtained in ref. 50 and 51. In addition, the gold nanoparticles exhibit a rich surface chemistry and allow one to conjugate various types of targeted analytes on the particles surface for enhanced selectivity binding to the substrate. They also enable one to real-time monitor the mass change effect when the bioconjugated gold nanoparticles are interacting with the substrate during the binding events.[52–56] All these unique features from gold nanoparticles enable them to serve as excellent candidates for amplifying the SPR sensing signals.[16,57] In the next few sections, we will first discuss different examples of using Au NPs that are composed of only element gold as amplification tags for enhanced SPR sensing of a variety of biological and chemical species and then provide an overview about the new development of enhanced SPR sensing techniques using gold nanocomposites (Au NCs) such as Au core–shell nanostructures.

2.1 Enhanced SPR sensing based on gold nanoparticles (Au NPs)

Over the past decade, the Au NPs-enhanced SPR systems have been extensively investigated since the first demonstration by Natan's group in 1998.[52,58–62] The group reported that a detection limit of 6.7 pM for human immunoglobulin G (h-IgG) and 25-fold signal enhancement were achieved by flowing functionalized Au NPs solution to the sensing surface when comparing to conventional PSPR sensors.[58] For sensing of lower molecular weight biological and chemical analytes with Au NPs enhanced SPR sensor, sandwich detection format is usually employed to improve the specificity and the limit of detection (LOD).[58,63] Typically, the targeted analytes are first flowed onto the SPR sensing film that is initially modified with capture receptors followed by flowing the solution of Au NPs functionalized with detecting agent.[17] In this way, sandwich structures with targeted analytes between the Au NPs and the sensing film are formed. A detailed summary of the investigated and studied targeted analytes (*e.g.* DNA, oligonucleotides, proteins, hormones, harmful chemicals in food and the environment) using Au NPs-enhanced SPR sensors is presented in Table 1.

2.1.1 Sensing of DNA and oligonucleotides. Detection of DNA and RNA sequence variations plays a key role in rapid clinical diagnosis of genetic-related diseases.[64,65] Although many kinetic studies based on conventional PSPR sensors for monitoring interactions between DNA molecules have been carried out in the past few decades,[66–68] there remains a huge challenge of detecting short sequence biomolecules such as oligonucleotides or single-base mismatch DNA because weak refractive-index changes can hardly be detected during the binding process. The first demonstration of Au NPs-enhanced SPR for sensing of DNA hybridization was reported by He *et al.*[52] The Au NPs were functionalized with oligonucleotide probes and they were able to selectively recognize the target DNA sequences. Through sequence-specific hybridization, a sandwich-like structure was formed in the reaction process where the targeted oligonucleotides were ''squeezed'' between the Au NPs and the Au sensing film. In their experimental setup, the authors have employed a home-built SPR imaging device with a macroscopic 4 × 4 array as the Au NPs-enhanced sensing platform and they were able to achieve a detection limit of 10 pM for 24-mer oligonucleotides (surface density $\leq 8 \times 10^8$ molecules per cm^2). This detection limit value has been significantly improved by at least 1000-fold in comparison to the unamplified binding detection scheme. It is also worth noting that this detection limit value is comparable to the detection sensitivity of the standard fluorescence-based scanning gene chips. It was proposed that there are three main factors that contributed to the enhanced SPR signal: (i) the large surface mass loading of the DNA:Au conjugates, (ii) high dielectric constant of the Au NPs and (iii) efficient electromagnetic coupling between Au NPs and the Au sensing film. Using a similar detection scheme, Hayashida *et al.*[69] later optimized the length of Au NPs-functionalized DNA sequence probe and demonstrated a large dynamic detection range from 1 pM to 10 μM for the target DNA molecules. They investigated and studied the binding efficiency of single-stranded DNA (ssDNA)-conjugated Au NPs probes with different DNA chain lengths (15-mer, 30-mer and 60-mer) and found that the 30-mer DNA–Au NPs probe achieved the best performance. Basically, a mercapto-acetic-acid (MAA) layer was initially formed on the Au thin film to prevent undesirable DNA absorbing onto the sensing surface. The change of SPR angle shift due to the hybridization interaction of DNA–Au NPs was determined to be 5 times larger than that of the one without functionalization of Au NPs. Recently, Moon *et al.*[70] further evaluated the use of a series of spherical Au NP (12 nm to 20 nm) for enhanced SPR detection of DNA hybridization based on a subwavelength Au nanograting

Table 1 Summary of Au-based nanoparticles amplified SPR sensors

Analyte	SPR sensor system	Enhancement strategy	Particle size	Limit of detection	Ref.
DNA and oligonucleotides					
Adenosine	Autolab SPR system	Colloidal Au NPs	13 nm	1×10^{-9} M	73
	Autolab SPR system	Colloidal Au NPs	13 nm	1×10^{-10} M	74
24-mer Oligonucleotides	Custom-built (angular reflectivity) & SPRI	Colloidal Au NPs	12 nm	10 pM	52
30-mer Oligonucleotides	Custom-built (angular reflectivity)	Colloidal Au NPs	10 nm	1 pM	69
39-mer Oligonucleotides	Custom-built FI–SPR (angular reflectivity)	Colloidal Au NPs	13 nm	1.38 fM	71
p53 cDNA	Custom-built FI–SPR (angular reflectivity)	Colloidal Au NPs	13 nm	100 fM	71
miRNA	Custom-built SPRI	Colloidal Au NPs	12 nm	10 fM	77
RsaI endonuclease	Custom-built FI–SPR (angular reflectivity)	Colloidal Au NPs	13 nm	5×10^{-8} M	80
Protein-immunoassay					
Human cardiac myoglobin	Biacore 3000	Colloidal Au NPs	6 nm	10 pM	133
Human IgE	Autolab SPR system	Colloidal Au NPs	13.9 nm	1 ng mL^{-1}	85
h-IgG	Custom-built (angular reflectivity)	Colloidal Au NPs	10 nm	30 nM	59
	Custom-built (angular reflectivity)	Colloidal Au NPs	11 nm	6.7 pM	58
	Custom-built (wavelength modulation)	Colloidal Au NPs	24 nm	0.30 μg mL^{-1}	120
	Custom-built (wavelength modulation)	Colloidal Au–Ag NCs	24 nm	0.15 μg mL^{-1}	120
SAH-IgG	Custom-built (angular reflectivity)	Colloidal Au NPs	40 ± 5 nm	300 nM	84
Bovine IgG	Custom-built (wavelength modulation)	GO sheets & colloidal Au NRs	58 × 24 nm	0.075 μg mL^{-1}	134
Rabbit IgG	Custom-built (wavelength modulation)	Colloidal Au NPs	23 nm	0.30 μg mL^{-1}	121
	Custom-built (wavelength modulation)	Colloidal ZnO–Au NCs	10 nm	0.15 μg mL^{-1}	121
Anti-rabbit IgG	Custom-built (phase detection)	Colloidal Au NRs	50 × 21 nm	40 pg mL^{-1}	17
Human IgM	Custom-built (wavelength modulation)	Colloidal Fe_3O_4–Au NCs	20 nm	0.30 μg mL^{-1}	23
Cholera toxin	NanoSPR-321	Colloidal Au NPs	17 nm	160 aM	89
Concanavalin A	Autolab SPR system	Colloidal Au NPs & GO-coated Au thin film	15 nm	0.39 μg mL^{-1}	135
Thrombin	Biacore X	Colloidal Au NPs	10 nm	0.1 nM	136
α-Fetoprotein	Autolab SPR system	Colloidal Fe_3O_4–Au NCs	25–30 nm	0.65 ng mL^{-1}	137
Transferrin	Custom-built (wavelength modulation)	Colloidal Au NRs & GO-coated Au thin film	65 × 25 nm	0.0375 μg mL^{-1}	138
Streptavidin	SPR-MACS (Moritex)	Colloidal Au–Al_2O_3 NCs	5.5 nm	5×10^{-10} M	116
	M-2000F spectroscopic ellipsometer	Au double-dots	90 × 100 nm	10 pM	91
Biotin	Custom-built (wavelength modulation)	Au NRs	380 × 25 nm	300 nM	14
Insulin-dependent diabetes mellitus – immunoassay					
Anti-GAD Ab	Biacore 2000	Colloidal Au NPs	21 nm	0.03 ng mL^{-1} (200 fM)	88
Cancer biomarker					
TNF-α antigen	Custom-built (phase detection)	Colloidal Au NRs	48 × 22 nm	0.03 pM	16
Pathogen					
S. typhimurium	Biacore 2000	Colloidal Au NPs	30 nm	10^4 cells per mL	87
Hormones					
Insulin	Autolab SPR system	Colloidal Au NPs	1.7 ± 0.3 nm	0.5 pM	107
Progesterone	Biacore 2000	Colloidal Au NPs	25 nm	8.6 pg mL^{-1}	53
	Biacore Q	Colloidal Au NPs	10 nm	4.9 ng L^{-1}	114
Testosterone	Biacore 2000	Colloidal Au NPs	25 nm	15.4 pg mL^{-1} – saliva matrix	54
Biocatalytic					
NAD^+ & NADH cofactors	Biosuplar-2	Colloidal Au NPs	2 nm	1×10^{-4} M	115
Chemical samples					
Explosive materials					
TNT	NanoSPR-321	Colloidal Au NPs	3.5 nm	10 fM	95
PETN	NanoSPR-321	Colloidal Au NPs	3.5 nm	200 fM	92
EGDN	NanoSPR-321	Colloidal Au NPs	3.5 nm	400 fM	92
Nitroglycerin	NanoSPR-321	Colloidal Au NPs	3.5 nm	20 pM	92
Alkaline-earth metal ions					
Mg^{2+}	NanoSPR-321	Colloidal Au NPs	4 nm	20 fM	97
Ca^{2+}	NanoSPR-321	Colloidal Au NPs	4 nm	40 fM	97
Sr^{2+}	NanoSPR-321	Colloidal Au NPs	4 nm	20 fM	97
Ba^{2+}	NanoSPR-321	Colloidal Au NPs	4 nm	1 fM	97

Table 1 (*continued*)

Analyte	SPR sensor system	Enhancement strategy	Particle size	Limit of detection	Ref.
N-Methyl carbamate inhibitors – insecticides					
C1 (513 Da)	Autolab SPR system	Colloidal Au NPs	15 nm	7 pM	98
C2 (585 Da)	Autolab SPR system	Colloidal Au NPs	15 nm	12 pM	98
Antibiotics – food					
Neomycin (NE)	NanoSPR-321	Colloidal Au NPs	3.5 nm	2.00 ± 0.21 pM	96
Kanamycin (KA)	NanoSPR-321	Colloidal Au NPs	3.5 nm	1.00 ± 0.10 pM	96
Streptomycin (ST)	NanoSPR-321	Colloidal Au NPs	3.5 nm	200 ± 30 fM	96
Enrofloxacin (ERFX)	SPReeta system	Colloidal Au NPs	19 nm	0.07 μg L^{-1}	139
Toxin – food					
Ochratoxin A	Biacore X	Colloidal Au NPs	27 ± 5 nm	60 pg mL^{-1}	99

patterned-sensing film. In this study, the SPR sensitivity for the detection of 24-mer ssDNA oligonucleotides (100 pM μL^{-1}) was enhanced by the coupling of LSPR excited on the nanogratings with SPPs on the Au sensing film and the coupling of LSPR excited on the Au NPs with the hybrid surface plasmon waves that were generated on the nanograting-patterned Au sensing surface. The nanogratings with a period of 300 nm, a fill factor of 67% and thickness of 10 nm were deposited on a 55 nm-thick Au sensing film using the lift-off method after they were patterned through electron beam (e-beam) lithography on a photoresist layer of polymethyl methacrylate (PMMA) followed by gold evaporation. During the SPR detection process, solution containing thiol-modified capture 24-mer ssDNA sequences which were complementary to the target 24-mer ssDNA sequences was firstly flowed onto the surface of Au nanograting patterned-sensing film followed by dispersion of Au NPs functionalized with the target 24-mer ssDNA sequences. A 57% signal enhancement was observed for the nanograting patterned-sensing film when compared to that measured using the control Au sensing film without nanograting patterns. According to the series of enhanced SPR measurements based on Au NPs with different diameters, the signal enhancement factors of Au NPs increased from 6.62-fold to 11.6-fold when the diameters of Au NPs (unified mass concentration) increased from 12 nm to 20 nm. The overall maximum signal enhancement was determined to be 18.2-fold when 20 nm Au NPs were used to couple with the nanograting patterned-sensing film. These obtained results also matched well with the corresponding theoretical analyses calculated by rigorous coupled-wave analysis (RCWA) and finite-difference time-domain (FDTD).

It was reported that the single-base mismatch and four mismatches in 39-mer targeted DNA sequences were respectively detected with high specificity and reproducibility by combination of using oligonucleotide-capped gold nanoparticle (ODN-capped Au NPs) sandwich assays and a custom-built high resolution microbore flow injection (FI) SPR setup.[71] More specifically, Yao *et al.* immobilized a carboxylated dextran film onto the sensing substrate surface to avoid any nonspecific adsorption of ODN-capped Au NPs. This Au NPs-enhanced SPR biosensing strategy has achieved a remarkable sensitivity of 1.38 fM for 39-mer oligonucleotides and 100 fM for polynucleotides-p53 cDNA with a reproducibility of relative standard deviation values less than 16%. It is worth mentioning that a bicell detector was employed in their SPR spectroscopy setup to obtain differential SPR signal for improving the stability of the sensing system. Separately, another group has shown that solely using this FI-SPR setup alone and in the absence of any functionalized Au NPs, a detection limit of 54 fM for 39-mer oligonucleotides can be obtained.[72] In addition to the sandwich detection scheme, Wang *et al.* developed[73,74] an indirect competitive inhibition assays (ICIA) using Au NPs–aptamer conjugates both as a competitive reagent and SPR signal amplification tags. Aptamers are generally divided into two categories: (i) nucleic acid aptamers and (ii) peptide aptamers, and they are promising substitute biomolecules and complementary counterparts for targeted analytes due to their straightforward synthesis process and discriminate recognition characteristic.[75,76] In this experiment,[74] the citrate-stabilized Au NPs with average diameter of 13 nm were modified with complementary antiadenosine-aptamers and the conjugates were used to hybridize with ssDNA molecules that were initially immobilized onto the SPR Au thin film. Further addition of a mixture solution to the sensing substrate that contained target adenosine and Au NPs functionalized antiadenosine-aptamers prevented the binding of Au NPs to the complementary ssDNA-modified sensing film since adenosine and antiadenosine-aptamers functionalized on Au NPs were hybridized and the entire ''nanocomplex'' was not able to recognize ssDNA molecules on the sensing interface, thus resulting in a dramatic decrease of the SPR signals when compared to that without adenosine in the solution (Fig. 3). The ICIA with Au NPs formulation showed good selectivity to adenosine in the presence of three other nucleoside-compounds (*e.g.* uridine, cytidine, and guanosine) and a sensitivity for adenosine of up to 1×10^{-10} M was obtained.

Besides short DNA sequences, small RNA molecules and even restriction endonucleases were also able to be detected using similar Au NPs-enhanced SPR schemes. MicroRNAs (miRNAs) are low-molecular-weight RNA molecules with only 19- to 23-mers and they have a great impact on gene regulation in plants and animals. They are known to be involved in many biological processes such as cell proliferation and fat metabolism. Fang *et al.*[77] reported that the use of *in situ* Au NPs-amplified SPR imaging technique for sensing of the mouse miRNA molecules and a detection limit of 10 fM have been demonstrated by using this approach. In their experiment, locked nucleic acids (LNAs) were specifically chosen as strong binding agents for the three different target miRNAs (miR-16, miR-122b and miR-23b) obtained from mouse liver tissue. After the targeted miRNAs hybridized with the complementary LNAs that were initially

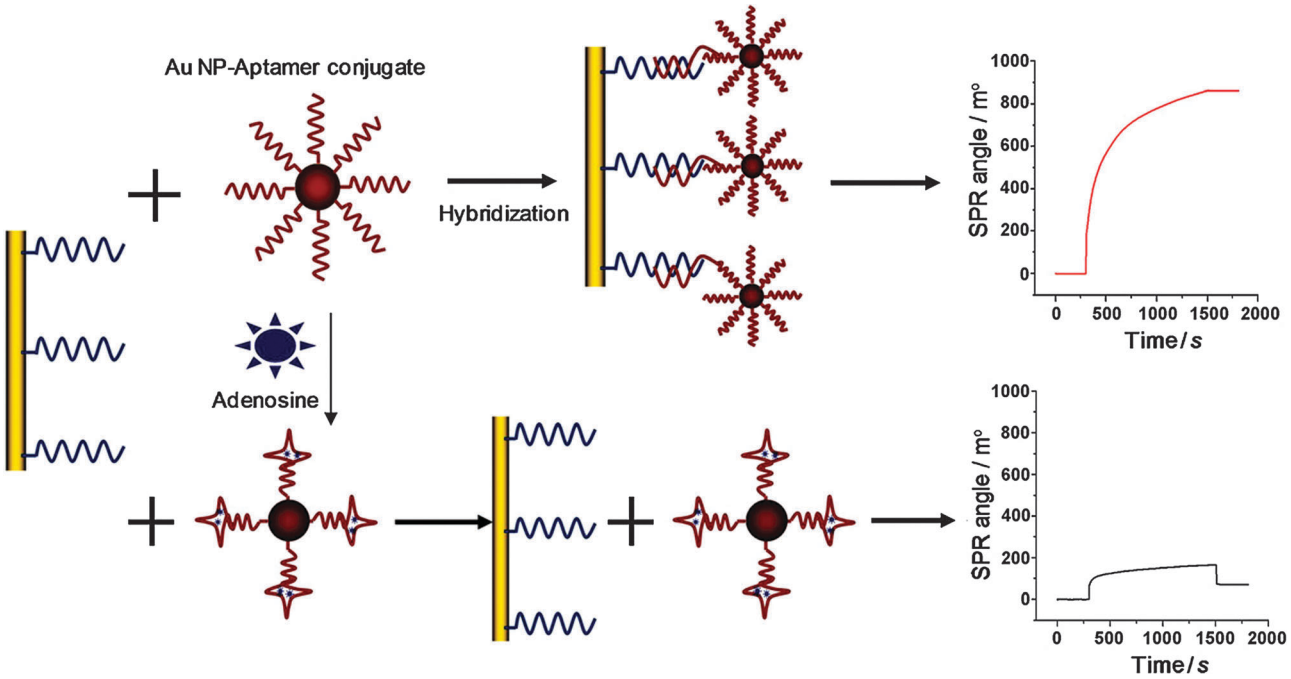

Fig. 3 Schematic representation of the SPR biosensor for the detection of adenosine that utilizes Au NPs–aptamer conjugates as a competitive reagent. Reproduced from ref. 74 with permission of Elsevier.

immobilized onto the microarray elements, poly(A) polymerase were added onto the array elements and tail-bound with miRNAs; finally functionalized Au NPs solution were then flowed onto the sensing surface and hybridized with poly(A) tails thereby resulting in a large SPR signal change. The use of poly(A) tails has effectively overcome the binding challenge of Au NPs to the short miRNA sequences.

Restriction endonucleases are important enzymes for genotyping, mapping and recombinant DNA technology.[78,79] Recently, Luan *et al.*[80] reported a novel Au NPs-amplified SPR strategy for sensing of RsaI endonuclease (5×10^{-8} M) without the effect of nonspecific adsorption. RsaI endonuclease is known for specifically recognizing the GTAC sequence and cleaving between the T and A. The entire detection process was based on an inhibition scheme (Fig. 4). First, the SPR sensing film was modified with DNA probes and hybridized with their complementary DNA sequences that were labeled onto Au NPs. Next, the RsaI endonuclease solution was flowed to the sensing surface leading to cleavages of the double-stranded DNAs and thus causing a significant decrease of the SPR signals when unbound Au NPs were flushed away from the substrate. The residual probe-DNAs left on the sensing surface were designed to be hairpin DNAs so that they could form stem–loop structures with good stability. It was shown in the control experiments that the large conformation changes of residual probe-DNAs also contributed to the SPR signal amplifications.

2.1.2 Protein detection. Immunoassays based on protein biomarkers and antibodies are crucial for preclinical and clinical studies because they can be used to quantitatively measure the amount of antigens in the serum samples through a protein complexing or decomplexing process.[14,81] The complexing or decomplexing process of protein is similar to the hybridization and dehybridization process between ssDNAs. However, many of the protein biomarkers and their complementary antigens either have a small molecular weight (less than 8 kDa) or they are extremely low-abundance (less than 1 pM) in the human serum.[82,83] Due to these reasons, conventional PSPR sensors are not sensitive in a dynamic detection range to detect this "special" group of biomolecules in the human serum since they are initially designed for monitoring large proteins–protein (more than 150 kDa) interactions. To overcome this challenge, Lyon *et al.*[58,59] have developed an Au NPs-enhanced SPR sandwich immunosensing method for detecting such types of biomolecules and they have demonstrated the concept by using picomolar human immunoglobulin G (h-IgG) as the study model. In this method, colloidal Au NPs were functionalized with secondary antibodies – Fc-specific monoclonal goat anti-human immunoglobulin G [a-h-IgG (Fc)] and acted as signal amplification labels. A 25-fold increase in the SPR sensitivity was achieved in comparison to that using the unlabeled sandwich immunoassay [a-h-IgG (γ)/h-IgG/a-h-IgG (Fc)]. Moreover, with the use of functionalized Au NPs, the sensing surface did not require to be initially modified by a dextran matrix which is commonly applied in conventional PSPR sensors for increasing the surface loading of the target analytes and decreasing the nonspecific adsorption of the biomolecules. They also experimentally demonstrated that increasing the diameter of the Au NPs from 25 to 60 nm had led to a larger SPR signal shift and a larger minimum reflectivity when the particle density remained the same. Later, the key role of functionalized Au NPs for signal enhancement on SPR immunosensing was further investigated by Gu *et al.*[84] They studied the same type of target analyte – human IgG along with an inhibition detection scheme instead of using the sandwich

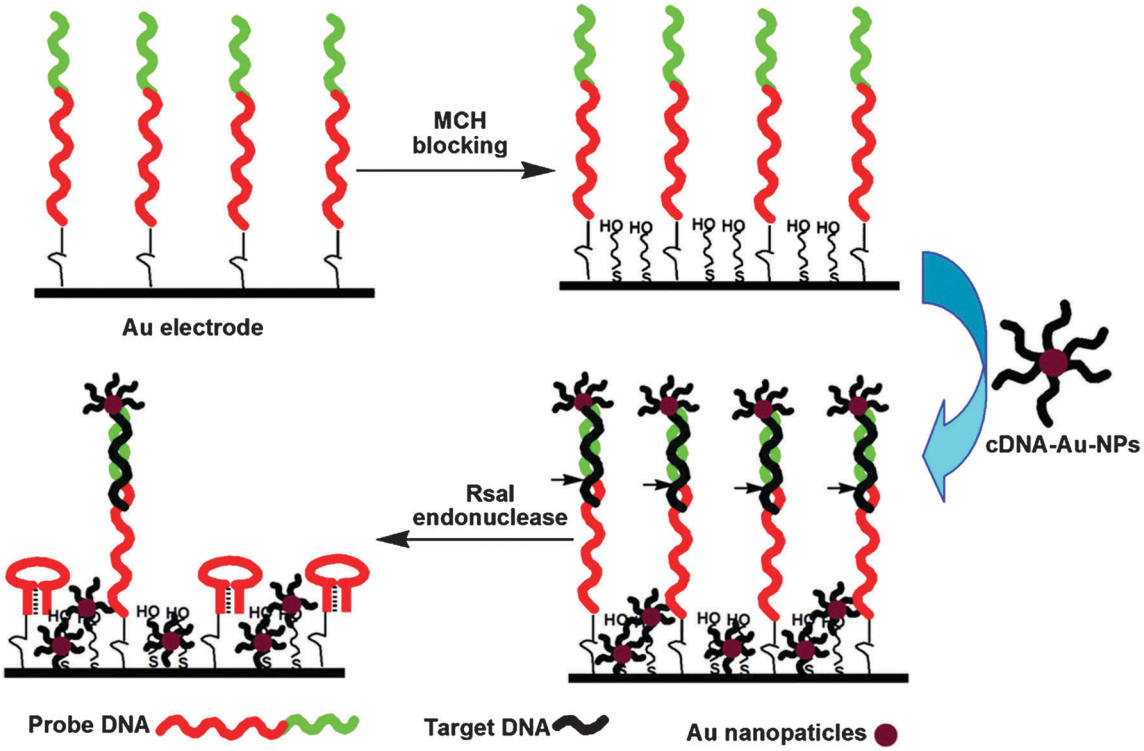

Fig. 4 Principal scheme of monitoring activity of RsaI endonuclease with the coaction of Au-NPs and hairpin DNA. For clarity, all of the molecules were not drawn to scale. Reproduced from ref. 80 with permission of Elsevier.

structure approach. The gold sensing film was initially immobilized with Fab′ fragments of human IgG molecules that would specifically interact with sheep–anti-human IgG (SAH–IgG). In the reference sensing process, the binding between the Fab′ fragments and SAH–IgG labeled Au NPs resulted in a large SPR signal change. In the detection sensing process, the mixtures of target human IgG (100 nM to 200 mM) and SAH–IgG:Au NPs were added onto the sensing surface and the presence of target human IgG reduced the binding between SAH–IgG:Au NPs and the Fab′ fragments at the sensing surface thus leading to a weaker SPR signal change. The maximum enhancement factor for the relative signal change by Au NPs was determined to be 300. Human immunoglobulin E (IgE), an antibody that plays a pivotal role in manifesting allergic diseases such as food allergy, allergic rhinitis and asthma, has also been investigated using Au NPs-enhanced SPR sensors.[85] The serum IgE concentration is generally known to be below 1 nM and direct detection of these molecules is hard to achieve using common PSPR sensors or other sensing devices.[86] Wang *et al.*[85] developed a typical sandwich detection approach for enhanced sensing of low-concentration human IgE (1 ng mL^{-1}) where Au NPs functionalized with 5′-thiol-modified aptamers were applied in the sensing scheme. The aptamer–Au NPs conjugates showed the advantages of reversible thermodynamic denaturation and better long-term stability against other antibodies labeled Au NPs. Moreover, nonspecific adsorption of SPR signal induced by aptamer–Au NPs conjugates was effectively minimized after 8 hours of pretreatment of the conjugates formulation with 6-mercaptohexan-1-ol (MCH). Unlike the enhanced SPR schemes that utilized antibody-labeled Au NPs for detecting human immunoglobulins, Ko *et al.*[87] demonstrated the design of a label-free enhanced SPR sensing approach that relies on the self-assembly of Au NPs onto 2-aminoethanethiol (AET)-modified Au sensing film. In this approach, citrate-stabilized Au NPs with an average diameter of 30 nm were initially assembled onto the sensing chip with an optimal coverage density of 1×10^9 particles per cm^2. Then, a fusion protein was used as an effective crosslinker to maintain the oriented immobilization of capture antibodies onto the Au NPs-assembled sensing surface. The fusion protein (GBP-ProA) was formed by genetically fusing gold binding polypeptides (GBP) to the N-terminal staphylococcal protein A (ProA) and bound to the Au NPs for reducing the steric hindrance of the later immobilized capture antibodies – 100 μg mL^{-1} human IgGs. When the Au NPs/GBP-ProA/hIgG-modified sensing surface was exposed to solutions containing 150 μg mL^{-1} target anti-hIgG, a 92% higher signal increase was obtained when compared to the signal that was measured using unmodified sensing chip. To further demonstrate the enhancement effect of Au NPs-assembled SPR sensing chip, solutions containing various concentrations of another target analyte – *Salmonella typhimurium* (*S. typhimurium*) – ranging from 10^4 to 10^6 cells per mL were flowed onto goat anti-IgG/GBP-ProA modified surfaces of both the unmodified chip and Au NPs-assembled sensing chip. The authors have observed that the detection limit for the *S. typhimurium* sample using Au NPs-assembled sensing chip was 10-fold lower than that using the unmodified sensing chip.

Cao *et al.*[88] reported a double SPR signal enhancement strategy using the Au NPs formulation for sensing of anti-glutamic acid decarboxylase antibody (anti-GAD Ab), which is an important indicator in the sera for diagnostics of insulin-dependent diabetes mellitus (IDDM) (Fig. 5). Basically, Au NPs were functionalized by HS-OEG_3-COOH and then covalently conjugated with horseradish peroxidase (HRP) and anti-IgG antibody in order to form an enzyme–immunogold complex (Au NPs–anti IgG–HRP), while the SPR sensor chip was modified by biotinylated GAD and interacted with the target anti-GAD Ab which resulted in a weak SPR signal change. The first amplification effect occurred after the injection of Au NPs–anti IgG–HRP complex onto the reactive sensing surface where the Au NPs acted as amplification tags upon the interactions between anti-IgG and the target anti-GAD Ab, which is a typical sandwich detection approach. The second amplification effect was achieved by further injecting DAB–H_2O_2 solution to the system, leading to the deposition of oxidized insoluble product on the SPR sensing surface. When both gold amplification and enzyme precipitation occurred, a detection limit of 0.03 ng mL^{-1} (or 200 fM) for anti-GAD Ab was achieved by using this technique. Another double SPR signal enhancement strategy based on Au NPs and *in situ* polymer growth was proposed and demonstrated for detecting attomolar bacterial cholera toxin (CT).[89] In this approach, citrate-stabilized Au NPs were first functionalized with hydroxyl and biotin groups and then linked with initiators of atom transfer radical polymerization (ATRP) that could trigger the localized growth of a poly(hydroxyl-ethyl methacrylate) (PHEMA) brush. They have also calcinated the Au sensing film and established a supported bilayer membrane (SBM) on the film surface through direct fusion of phosphatidylcholine (PC) vesicles. The vesicle solutions were prepared in advance by mixing PC lipid stock solution with a portion of stock solution of cell receptor monosialoganglioside GM1 and then injected onto the sensing film to allow the fusion to take place. The embedded GM1 in the SBM was capable of capturing the target CT molecules. During the detection process, solutions containing target CT with different concentrations (630 aM to 590 nM) were flowed to the PC/GM1-modified sensing surface and then followed by 0.25 mg mL^{-1} biotinylated anti-CT, 0.2 mg mL^{-1} avidin, dispersion of AuNP–initiator–biotin, and finally mixture of HEMA/catalyst that would trigger the ATRP reaction on the surface of Au NPs. Thus, a sandwich immunoassay with target CT trapped between GM1 and Au NPs was formed. The first signal enhancement was attributed to the

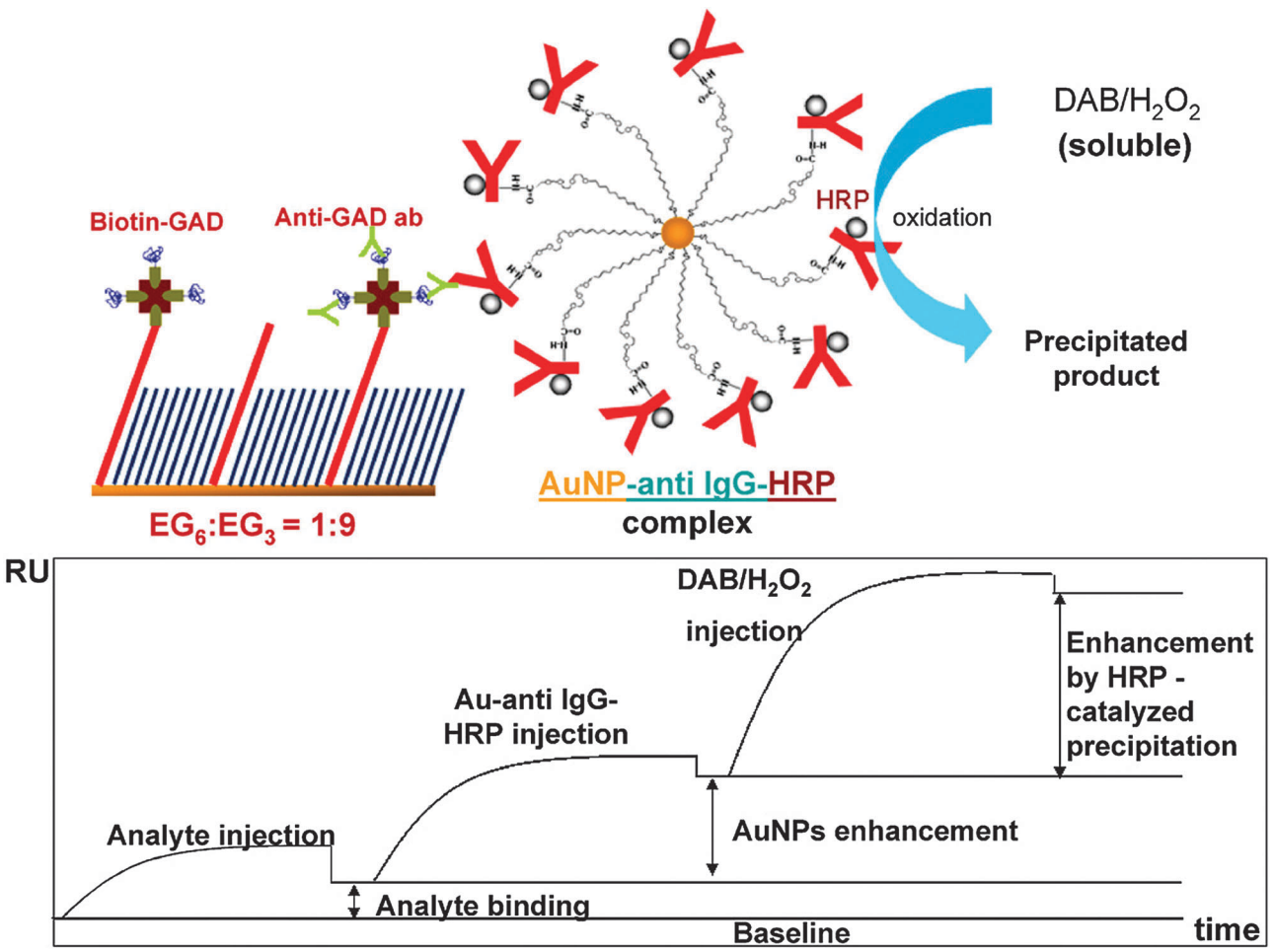

Fig. 5 Schematic diagram illustrating the steps in anti-GAD Ab detection and enhancement strategy based on the SPR immunosensor. Reproduced from ref. 88 with permission of Elsevier.

coupling of Au NPs to the sensing interface as amplification tags, and the second signal enhancement was due to the inline ATRP polymer growth of PHEMA brush that induced large mass perturbations on the surface. The detection limit of this enhanced SPR approach using Au NPs and their assisted ATRP reactions for target CT was 160 aM, which was 9 orders of magnitude lower than that obtained using the conventional SPR measurement method.

Recently, our group has incorporated functionalized gold nanorods (Au NRs) into a home-built phase-sensitive SPR sensor as amplification labels for detection of trace-amounts of anti-rabbit IgG (40 pg mL^{-1})[17] and tumor necrosis factor alpha (TNF-α) antigen (0.03 pM).[16] During the sensing process of anti-rabbit IgG, the wavelength of excitation light source was fixed at 785 nm.[17] Au NRs with different aspect ratios (NR-530, NR-642, NR-718 and NR-772) but with same concentration were conjugated to the target anti-IgG and then interacted with IgG immobilized onto the sensing film, respectively. The enhancement factors of Au NRs to SPR signals have been studied and compared under the same detection conditions. The maximum enhancement effect was obtained when NR-642 sample was employed as the amplification label. It was found that NR642–anti-IgG sample has the maximum enhancement effect and this effect was related to a function-based relation between the LSPR peak wavelength of Au NRs and the wavelength of the excitation light source. Simulation results using finite element analysis (COMSOL Multiphysics 3.5) further confirmed that this enhancement was due to the coupling effect between the nanorods and the Au sensing film. The detection limit for anti-rabbit IgG was determined to be 40 pg mL^{-1}, which is 23 times more sensitive than that without using Au NRs as labels. The Au NRs-enhanced SPR effect was also reported by Hao *et al.*[90] In their study, Au NRs were functionalized with the polyelectrolyte polymer for conjugating the target rabbit anti-goat IgG thereby allowing them to be captured by goat IgG antibodies that were initially immobilized onto the sensing film. The binding process was monitored through a custom-built SPR sensor based on a wavelength-modulation mode. Later, the same principle was extended by our group for the detection of TNF-α antigen that is an endogenous tumor promoter for the early-stage development of cancer and the antigen has a small molecular weight of 17 kDa.[16] Au NRs with a dimension of 48 nm × 22 nm were specifically chosen based on our theoretical modeling results and the particles were conjugated with anti-human TNF-α antibody. The absorption peak of the Au NRs was around 645 nm and it was closely matched to the wavelength of laser source at 785 nm in order to obtain the maximum signal enhancement. TNF-α antigen solution were injected and reacted with the capture antibodies immobilized onto the sensing film. Subsequently, the secondary antibodies-conjugated Au NRs solution is flowed to the system and interacted with the ''captured'' antigens on the substrate. Thus, a sandwich immunoassay with target TNF-α antigen between Au NR and the Au sensing film was formed. The detection limit for TNF-α was estimated to be 0.5 ng mL^{-1} (0.03 pM) and a 40-fold enhancement was observed in comparison to the unlabeled SPR detection scheme under similar conditions.

More recently, Kravets *et al.*[91] reported the design of a novel and flexible enhanced SPR sensing film that consisted of Au nanoarrays with diffractive coupling of localized plasmon resonances (DCLPR) exhibiting high phase sensitivity for single-molecule detection (Fig. 6). The excitation of SPR in this plasmonic metamaterial system is similar to that of the conventional PSPR sensors which is through attenuated total reflection geometry by a visible light source. The resonance angle and wavelength can be tuned by manipulating the periodicity of the nanoarrays. Several array structures have also been investigated including nanodots (dot diameter ~100 nm, thickness ~90 nm, array period ~300 nm), double dots, Au dumbbells, stripes and arrays of holes in PMMA–Au double layers. It was found that the double dot structure showed the highest quality factor and they have more versatile control over the resonance position from the ellipsometric measurements when 10 pM streptavidin was tested as the target analyte in the system.

2.1.3 Detection of harmful chemicals for food and environmental monitoring. Precise identification and quantification of harmful chemicals like residual antibiotics in meat or dairy products, pesticides in vegetables and explosives such as trinitrotoluene in water or soil are highly desired from the perspective of healthcare, environmental monitoring and homeland security.[92] Trinitrotoluene (TNT) is a small molecule with a molecular weight of 227.13 Da. Ultrasensitive detection of TNT is important for preventing possible terrorist attacks and monitoring contaminations in munitions wastewater or on sites of former military installations.[93,94] Riskin *et al.*[95] reported an amplified SPR sensing strategy with a detection limit of 10 fM for TNT molecules by electropolymerizing a bis-aniline-cross-linked Au NPs composite on the sensing surface as the enhanced binding matrix (Fig. 7). More specifically, Au NPs with an average diameter of 3.5 nm were functionalized with a mixed monolayer of thioaniline and mercaptoethane sulfonate and served as signal amplification tags during the sensing process. To generate the enhanced TNT binding sites, a molecular imprinting method was used in this work. Basically, thioaniline-functionalized Au NPs were first electropolymerized onto the surface of Au sensing film as imprinted sites and then picric acid, an analogue for TNT, was injected to form π-donor–acceptor complexes; finally picric acid imprint molecules were removed by immersing the modified sensing film in a 0.1 M HEPES solution and thus leaving the π-donor sites for interacting with the target TNT molecules. Both experimental and theoretical results have shown that this molecular-imprinted matrix owned a high binding affinity to TNT with an association constant up to 6.4×10^{12} M^{-1} which led to large SPR signal changes. Later, the same group[96] employed a similar SPR signal amplification principle for targeted sensing of three antibiotic analytes: neomycin (NE), kanamycin (KA), and streptomycin (ST) in milk samples. In this study, Au NPs were functionalized with thioaniline as electropolymerizable units, mercaptoethane sulfonate as stabilizing caps, and (mercaptophenyl)boronic acid as an active ligand to bind to the antibiotics that have the vicinal diol functionalities. The binding between boronic acids and the antibiotics is reversible and the binding will dissociate under acidic conditions (pH 1.3) and re-associate again under basic conditions (pH 9.2 in buffer solution). Thus, after the electropolymerization

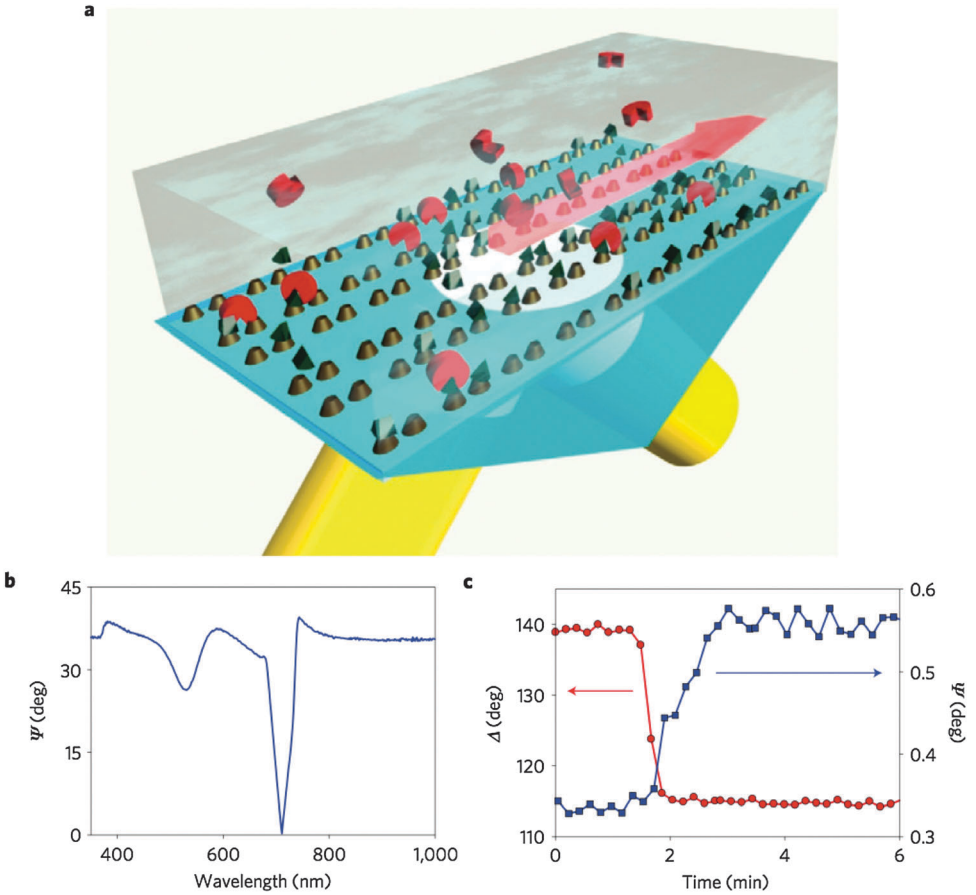

Fig. 6 Enhanced SPR biosensing with a plasmonic metamaterial based on Au nanodot arrays. (a) Typical schematics of measurements. The dark green triangles represent biotin, the red disks represent streptavidin. Light beams are shown in yellow, the grazing diffracted wave is shown by the red arrow. The double dot array used in biosensing experiments has the following parameters: array constant a = 320 nm, average size of the dots d = 135 nm and dot separation of the pair s = 140 nm. (b) Ψ *versus* wavelength for an incidence angle of 53°. (c) Evolution of Δ and Ψ with time as streptavidin molecules bind to functionalized Au dots, measured at λ = 710 nm and θ = 53°. Reproduced from ref. 91 with permission of Nature Publishing Group.

of Au NPs on the Au sensing surface, the imprinted bisaniline-crosslinked Au NP composites were formed through the injection of ligated antibiotics buffer solution and these ligated antibiotics were then removed from the Au NPs composite matrix through acidic immersions in order to generate structural contours for enhanced binding of the target antibiotic analytes. The detection limit using this method for sensing of NE, KA and ST in buffer solution were demonstrated to be 2.00 ± 0.21 pM, 1.00 ± 0.10 pM and 200 ± 30 fM, respectively. By using 5000-fold diluted milk as sample solution, 10 pM NE, 52 pM KA and 28 pM ST were detected with high selectivity for each respective antibiotic analyte. More recently, Ben-Amram *et al.*[97] extended the application of this Au NPs-enhanced imprinting SPR approach for detecting alkaline-earth metal ions (*e.g.* Mg^{2+} (20 fM–200 pM), Ca^{2+} (40 fM–100 pM), Sr^{2+} (20 fM–200 pM) and Ba^{2+} (1 fM–25 pM)) by replacing the active ligand on the functionalized Au NPs with dithiothreitol molecules. The imprinted sites showed high selectivity to the specific types of alkaline-earth ions. The authors also suggested that this proposed imprinting method would be useful in the development of SPR sensors for environmental monitoring of toxic metal ions such as Cr^{6+} or $As^{3+/5+}$.

N-Methyl carbamate inhibitors (molecular weight less than 600 Da) are widely used insecticides for agricultural plants and they can also be identified through Au NPs-enhanced SPR sensing strategy even at a concentration as low as the picomolar level. Huang *et al.*[98] investigated the specific binding interactions between Au NPs-labeled carbamate inhibitors (ALC1 and ALC2) and their targets – acetylcholinesterase (AChE) molecules using a commercial Autolab SPR system. The Au sensing film was initially modified with a self-assembly monolayer of 11-mercaptoundecanoic acid (MUA) and followed by the immobilization of AChE through an amide bond. A fixed amount of the lipoate moiety was linked to the two carbamate inhibitors for enabling their binding to the Au NPs. The concentration of Au NPs was optimized by evaluating the Au NPs functionalized with 0.6 nM carbamate inhibitor 1 (C1) formulation with different concentrations ranging from 4.8 to 48 mg L^{-1} and they were bound to the immobilized AChE onto the SPR sensing surface for determining the best signal enhancement. It was reported that the maximum signal change was obtained by Au NPs at 24 mg L^{-1}. A detection limit of 7 pM for C1 (513 Da) and 12 pM for C2 (585 Da) was achieved with Au NPs at the fixed optimal concentration, while no observable SPR signal change was

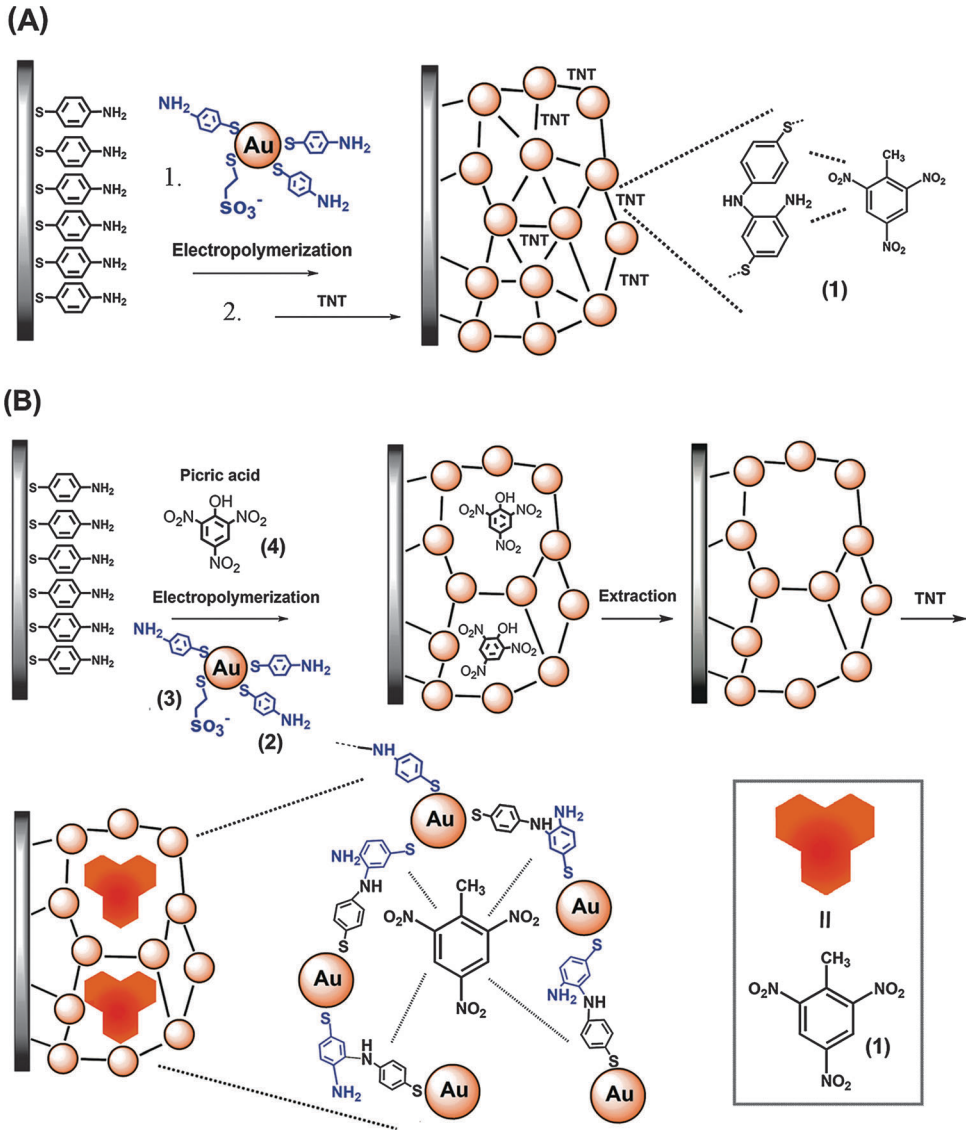

Fig. 7 Schematic diagrams for (A) electropolymerization of a bis-aniline-crosslinked AuNPs composite for the SPR sensing of TNT by donor–acceptor interactions; (B) imprinting of TNT molecular recognition sites into the bis-aniline-crosslinked AuNPs composite associated with a Au sensing film. Reproduced from ref. 95 with permission of The American Chemical Society.

induced for C1 even at a high concentration of 0.6 nM under similar conditions without Au NPs as labels. Another type of analyte called ochratoxin A (OTA) that belongs to a group of mycotoxins produced by aspergillus/penicillium species often contaminates agricultural commodities and has strong toxic effects on the liver and kidneys of both humans and animals. Recently, it was demonstrated that Au NPs-enhanced SPR sensing approach can be used to detect OTA with sensitivity as low as 60 pg mL^{-1}.[99] Basically, Urusov *et al.* functionalized the citrate-stabilized Au NPs (27 ± 5 nm) with anti-species antibodies (peroxidase-labeled anti-mouse IgG) instead of unmodified specific antibodies (native anti-mouse IgG antibodies) to reduce the amount of un-reacted unmodified specific antibodies during the sensing process and thereby effectively reduced the signal noises from the background. The Au sensing film was initially modified with bovine serum albumin (BSA) and OTA (with the molar ratio of 1 : 15) at an optimal concentration of 100 μg mL^{-1}. During the detection process, the 1 : 1 immune mixtures of unmodified specific antibodies at a fixed concentration of 50 ng mL^{-1} and target OTA solutions with various concentrations ranging from 60 pg mL^{-1} to 500 ng mL^{-1} were flowed onto the OTA–BSA modified sensing surface, followed by flowing dispersion of Au NPs functionalized with anti-species antibodies. The un-reacted sites of the unmodified specific antibodies that were available after the competitive interaction process would bind to the OTA that was previously immobilized onto the sensing film. Thus, the increase concentration of the target OTA in the mixture solutions led to a decrease of the SPR sensing signal. The anti-species antibodies immobilized onto the Au NPs would then bind with another end of the unmodified specific antibodies and result in an enhanced signal change of 10-fold and 3-fold when compared to that without Au NPs and

with Au NPs functionalized with unmodified specific antibodies. In this study, the SPR detection limit was lowered from 0.4 ng mL^{-1} to 60 pg mL^{-1} which is an order of magnitude difference in the sensitivity response.

2.1.4 Detection of hormone and other biologically-related molecules. The development of real-time and ultrasensitive sensors for detecting hormones such as insulin, progesterone and testosterone has been a major research thrust in the past few years.[100–102] Sensing of insulin in serum plays a key role in clinical diagnostics for various types of diabetes and anti-doping control for athletes.[103–106] Frasconi *et al.*[107] demonstrated an enhancement method for SPR detection of trace-amount insulin in human serum using colloidal Au NPs conjugated with poly(amidoamine) G4-PAMAM dendrimers as an amplifying nanoplatforms (Fig. 8). The surface coverage of Au NPs was carefully tailored by dendrimer density during the functionalization process of preparing the dendrimer-encapsulated Au NPs formulation. Thus, the coupling effect between localized SPR of Au NPs and surface plasmon wave generated on the Au sensing film was easily optimized for enhanced sensing use. In addition, the dendrimer thiol groups on the Au NPs surface would enhance the immobilization of capture insulin onto the surface of the dendrimer-encapsulated Au NPs. The detection process was based on an indirect competitive immunoassay scheme where the target insulin solutions with different concentrations (0.5–86 pM) were mixed with anti-insulin antibodies (Ins-Abs) at a fixed concentration (0.8 nM) and subsequently the mixtures were flowed onto AuNP-G4-OH-modified SPR sensing surface and reacted with the capture insulin which were initially immobilized onto the surface of dendrimer-encapsulated Au NPs. The SPR sensing signal was observed to decrease upon increasing the concentration of the target insulin. It was demonstrated that the detection limit for insulin in serum samples using this strategy could achieved at concentration as low as 0.5 pM. Different from water-soluble peptide hormones like insulin, progesterone and testosterone are two fat-soluble and water-repellent steroid hormones.[108,109] They are important biomarkers for indicating physiological changes of reproductive systems.[110,111] For instance, mammalian estrous cycles and ovarian diseases can be reflected and monitored from the plasma progesterone levels.[112,113] Mitchell *et al.*[53] reported the detection of progesterone at an unusual dilute concentration of 8.6 pg mL^{-1} in buffer solution by employing 25 nm Au NPs-labeled secondary antibodies conjugate in the SPR enhancement immunoassay system. The dextran sensor surface of commercial Biacore 2000 was modified by progesterone coating antigens using oligoethylene glycol (OEG) linkers through 4-position binding instead of conventional 7-position one. In this study, anti-rat IgG served as the secondary antibody for conjugation with the Au NPs and a fix concentration of IgG (800 μg mL^{-1}) as the inhibition assay was maintained for all the experiments. The sequential binding scheme with Au NPs labeling possessed an obviously improved detection sensitivity (8.6 pg mL^{-1}) in comparison to that of the prelabeling scheme with the biotinylated monoclonal antibody alone – 143 pg mL^{-1} and secondary antibody without being labeled to NPs – 20.1 pg mL^{-1}. More recently, the same group[54] used a similar approach to detect testosterone, which is another type of anabolic steroid hormone and a principal sex hormone for males. A 12.5-fold signal sensitivity was increased in the case of application of Au NPs-labeled the secondary antibody for sensing the testosterone molecules compared to that by solely using a primary antibody. Based on this approach, the detection limits for testosterone in buffer solution and human saliva matrix were shown to be 3.7 pg mL^{-1} and 15.4 pg mL^{-1}, respectively.

The SPR immunoassay system for detecting progesterone was later improved by Yuan *et al.*[114] where they used both IgG–Au NPs (10 nm) as amplification tags and a highly stable sensor surface with mixed self-assembled monolayers (mSAM) modified by protein conjugates (P4–OEG–OVAs) to demonstrate their concept. The protein conjugate (P4–OEG–OVA) was formed by conjugating progesterone (P4) with ovalbumin (OVA) and

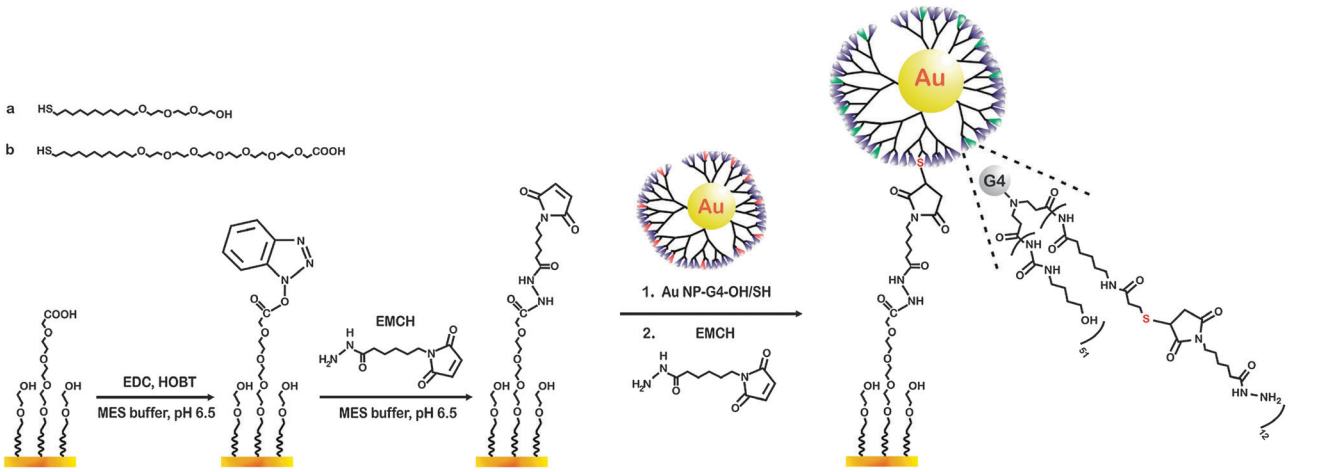

Fig. 8 Schematic illustration for immobilization of hydroxyl/LC-PDP-functionalized G4-PAMAM dendrimer-encapsulated Au nanoparticles onto mixed SAMs of alkanethiolates on gold derived from tri(ethylene glycol)-terminated thiol (a) and the hexa(ethylene glycol) carboxylic acid-terminated thiol (b). Reproduced from ref. 107 with permission of The American Chemical Society.

oligoethylene glycol (OEG). This modified mSAM surface was thinner than the commonly used dextran layer (100 nm) that shortened the interaction distance between Au NPs and the Au sensing film. Thus, a larger coupling effect at the gap could be obtained. The enhanced inhibition SPR detection process was performed by first injecting a mixture of anti-progesterone antibodies (mAbs) and target progesterone solution onto the mSAM/P4–OEG–OVA sensor surface, and then followed by introducing IgG–Au NPs (10 nm) solution at a fixed concentration. The SPR measurements using IgG–Au NPs (10 nm) have significantly reduced the required mAb concentration from 50 mg L^{-1} (non-enhanced assay) to 3 mg L^{-1}. More importantly, the detection limit for progesterone has been improved from 372.7 ± 77 ng L^{-1} (by a non-enhanced assay) to 4.9 ± 1.7 ng L^{-1} with the presence of Au NPs as amplification tags. Over 400 binding–regeneration cycles without baseline shift and ultrasensitive detection of antibody binding capacity within the system was demonstrated in this designed sensing approach due to the high stability of the mSAM/P4–OEG–OVA sensing surface.

In addition to DNA, protein and hormone, other biologically-related small molecule interaction can also be detected and analyzed using the Au NP-enhanced SPR sensing method. For example, NADH and NAD^+ cofactors, a type of metabolic molecules involved in redox reactions and attractive targets for drug designs, were detected by enhanced SPR sensing approach based on either electrochemical or biocatalyzed deposition of methyl-(aminopropyl) viologen-functionalized Au nanoparticles ($MPAV^{2+}$-Au NPs) on the Au sensing film.[115] These bipyridinium radical cation-functionalized Au NPs were prepared by conjugating *N*-(3-aminopropyl)-*N*′-methyl-4,4′-bipyridinium to the tiopronin-capped Au NPs (diameter *ca.* 2 nm). When NAD^+ was injected onto the Au NPs-modified SPR sensing surface in the presence of diaphorase (DP), NAD^+ cofactors were reduced and formed NADH thereby resulting the desorption of the functionalized Au NPs from the sensing film and leading to a large angular shift of SPR signal, while V^+ – Au NPs were oxidized into V^{2+} – Au NPs simultaneously. The process is reversible and thus both concentrations of NAD^+ and NADH could be detected. The sensing concentration for NAD^+ and NADH was ranged from 1×10^{-4} M to 2×10^{-3} M and 1×10^{-4} M to 1×10^{-3} M, respectively. These results demonstrated the potential of functionalized Au NPs with radical cation for SPR signal amplification since active electron from the radical can be transferred to the Au NPs surface thereby further enhancing the coupling effect between the LSPR and surface plasmon wave on the sensing film.

2.2 Enhanced SPR sensing based on gold nanocomposites (Au NCs)

In the last decade, ''pure'' gold nanoparticles (Au NPs) have been constantly used as signal amplification tags for enhanced SPR sensing of various small molecules as discussed in Section 2.1. Currently, many research groups are trying to incorporate other nanoparticles (*e.g.* semiconductor nanoparticles, metal nanoparticles, magnetic nanoparticles, *etc.*) into the single-element Au NPs formulation to form gold nanocomposites (Au NCs) and employ them for SPR detection applications. Thus, Au NCs here represent nanoparticles that are composed of not only gold element but also other metal elements such as silver and aluminum. Koshizaki's group[116] reported the design of the Au–Al_2O_3 nanocomposites modified SPR sensing film for ultra-sensitive detection of streptavidin. The deposited Au–Al_2O_3 nanocomposite films showed high stability and the average interparticle distances between Au NPs could be manipulated by varying the surface coverage of the Au NPs on the film. The dielectric matrix of Al_2O_3 on the Au NCs-modified sensing film can serve as a spacer and it can effectively reduce the steric hindrance and electrostatic repulsion that would occur during the binding process between target streptavidin molecules and biotin-functionalized Au NPs. In addition, the Au–Al_2O_3 nanocomposites modified sensing film can be readily used for sensing without the need for immobilization of Au NPs onto the substrate surface. The authors carried out all the experiments based on a commercially available SPR-MACS biosensor. Using this developed method, the detection limit of streptavidin was estimated to be 5×10^{-10} M when Au particle size of 5.5 nm, 45% surface coverage of NCs and an average interparticle distance of 3.8 nm were used in the experiments.

It is known that silver nanoparticles (Ag NPs) showed a stronger excited electric field enhancement effect and a deeper SPR resonance dip than that of the Au NPs when coupled to the SPR sensing film.[117–119] However, the major challenge to use Ag NPs in SPR sensing is that they are not stable and easy to be oxidized. To overcome this challenge, Song *et al.*[120] developed an Au–Ag alloy nanocomposites-amplified SPR immunoassay where the nanocomposites showed excellent resistance to oxidization and at the same time the engineered system demonstrated high sensitivity capability. The colloidal Au–Ag alloy nanocomposites (Au–Ag NCs) with an average size of 24 nm were fabricated using the same method described for citrate-stabilized Au NPs except by using a fixed molar ratio (0.27 : 0.73) of both gold and silver precursors during the synthesis process. The prepared Au–Ag alloy nanocomposites were then immobilized onto the gold sensing substrate that was initially functionalized with sulfhydryl groups. X-ray photoelectron spectroscopy (XPS) tests revealed that Au–Ag NCs were successfully immobilized onto the sensing film. In the experiment, human IgG was chosen as the target analyte model and a custom-built wavelength-modulation SPR biosensor was used for monitoring the protein binding interaction. Rabbit anti-human IgG was then functionalized onto the nanocomposites-modified thin film before injecting the target human IgG solutions to the sensing system. It was found that the Au–Ag alloy nanocomposites-based SPR sensor was able to response to the target human IgG with a detection range of 0.15–40.00 μg mL^{-1}, while SPR response based on Au NPs with same particle size as the NCs showed a much narrower concentration range of 0.30–20.00 μg mL^{-1}. The SPR detection range without nanoparticle-amplification for target human IgG was determined to be 1.25 to 20.00 μg mL^{-1}.

Later, the same group further developed a colloidal ZnO–Au nanocomposite-based SPR enhancement approach for ultra-sensitive sensing of rabbit IgG.[121] In general, ZnO nanocrystals are known to be colloidally unstable in aqueous solutions and

they are easily aggregated but ZnO–Au nanocomposites (ZnO–Au NCs) can be made water-dispersible, maintaining high colloidal stability even when they are exposed in the biological fluids.[122] More importantly, they have demonstrated that the energy transfer from the surface of excited ZnO nanocrystals to the surface of Au NPs led to a stronger electric field enhancement thus generating a higher SPR sensitivity in the system. In this experiment, ZnO–Au NCs with a particle size of 10 nm were first functionalized with target rabbit IgG and then the goat anti-rabbit IgG molecules were immobilized onto the surface of the SPR biosensor. During the experiment, the volume of ZnO–Au nanocomposites and concentration of goat anti-rabbit IgG were fixed at 0.25 mL and 75 μg mL^{-1}, respectively. Using these experimental parameters, the colloidal ZnO–Au nanocomposites-based SPR biosensor was able to detect rabbit IgG with concentration ranging from 0.15 to 20.00 μg mL^{-1}, whereas the conventional SPR biosensor based on solely 23 nm Au NPs achieved a much narrower concentration range, which is between 0.30 and 20.00 μg mL^{-1}. This detection method showed high selectivity to rabbit IgG from control SPR tests since no interactions were monitored when solutions containing human IgM and ZnO–Au–BSA were separately flowed onto the sensing substrate.

In addition to the nanocomposites mentioned above, core–shell Fe_3O_4–Au nanocomposites were synthesized and applied in the enhanced SPR sensing as well. Wang *et al.*[23] prepared Fe_3O_4–Au nanocomposites (Fe_3O_4–Au NCs) by coating the magnetic Fe_3O_4 nanoparticles with Au shells and investigated their effects on SPR sensitivity. The synthesized Fe_3O_4–Au NCs possess excellent magnetic properties and long-term colloidal stability as well as rich surface chemistry for versatile coupling of biomolecules. In this work, the chemical modification of the SPR sensing surface was achieved by depositing functionalized Fe_3O_4–Au NCs on the substrate surface with the aid from guided magnetic forces of a magnetic pillar. The diameters of Fe_3O_4–Au NCs can be tuned by changing the amount of 3-mercaptopropionic acid (MPA) during the synthesis process. The variation of MPA concentration in the reaction mixture will affect the total amount of MPA molecules adsorbed on the surface of Au shells thereby affecting the overall growth rate of NCs during synthesis process. Fe_3O_4–Au nanocomposites with diameters ranging from 8 to 30 nm were prepared in this study and they were functionalized with goat anti-human IgM for SPR sensing of human IgM molecules. The authors have shown that a wide detection concentration range of 0.30–20 μg mL^{-1} can be achieved for target human IgM molecules with the SPR biosensor based on 20 nm Fe_3O_4–Au NCs. On the other hand, a narrower concentration range of 1.25–20 μg mL^{-1} was obtained in the absence of the NCs.

2.3 Guidelines for designing gold nanoparticles-amplified SPR sensors

The studies of Au NPs-amplified SPR coupling effect were originally demonstrated in 1999 by Lyon *et al.*[59,60] and in 2004 by He *et al.*[61] They have experimentally found that larger SPR signal changes were observed when larger sizes of Au NPs (12–59 nm) were immobilized onto the Au sensing film with a fixed coupling distance of 3 nm (thickness of monolayer of 2-mercaptoethylamine). Such results have attracted great attention from the SPR community and since then many research groups have started to investigate and evaluate the size- and distance-dependent coupling effect of Au NPs on the SPR sensing film.[16,57,91] It is worth noting that the majority of the enhanced SPR sensing studies that are listed in Table 1 utilize Au NPs with an average diameter ranging from 10 to 20 nm in their experiments. Unfortunately, these sizes of Au NPs are not optimized for the best performance of SPR sensing since Au NPs size plays a crucial role in determining the enhanced sensitivity of the SPR system. Based on our analysis, there are two main reasons that might lead to the favorable use of 10 to 20 nm Au NPs for an enhanced SPR sensing study. Firstly, Au NPs dispersion with diameters ranging from 10 nm to 20 nm can be easily prepared in the laboratory (using standardized protocol) or purchased from the biotechnology companies, thus making them accessible to researchers with diverse backgrounds who are working on SPR sensing applications.[39] Secondly, the preparation of Au NPs with particle size larger than 30 nm is not as easy and straightforward as today when compared to ten years ago and this has forced the SPR community to continuously use 10 to 20 nm size of Au NPs for the development of Au NPs-amplified SPR sensors since the majority of the SPR researchers do not interface with the Au NPs chemistry in detail.[13] These factors are the main driving force that caused the SPR community to be stagnant in the use of 10 to 20 nm Au NPs for the corresponding sensing studies. To date, commercially available products of spherical Au NPs dispersion with diameters ranging from 1.8 to 125 nm with size accuracies of up to 0.1 nm and size variance less than 4% are currently obtainable from companies such as Nanopartz Inc. and Sigma-Aldrich and availability of such products has prompted many SPR researchers to initiate the investigation on the size effects of the Au NPs for enhanced SPR detection. Moreover, with the recent advancement in colloidal synthesis chemistry for preparing high-quality anisotropic Au NPs (*e.g.* nanorods, nanocubes, nanocages, nanoprisms, nanoplates, and dendrimer-like shapes),[123–126] optimizing the size and shape of Au NPs for specific enhanced SPR sensing of biomolecules are now possible to be studied and demonstrated.

In general, during the process of designing a particular type of Au NPs-amplified SPR sensing strategy, one needs to carefully consider and analyze four key components prior to performing the experiments: (i) the details of the target analyte (*e.g.*, concentration, molecular weight and structure of the molecules); (ii) the type of detection matrix used in the experiment (*e.g.*, water, buffer, human serum); (iii) chemical functionalization schemes needed for modifying the sensing film and Au NPs surface (*e.g.*, with thiol or amino reaction groups or capture counterparts of the target analyte); and (iv) the sensing mechanism employed for the study (it can be either a sandwich or a competitive inhibition sensing approach). After determining the four components, one can move to the next stage to select or optimize the structure/thickness of the SPR sensing substrate.

Although the commonly used 50 nm Au thin film-coated glass substrate for SPR sensing can be easily prepared by thermal evaporation deposition or commercially obtained from SPR-related companies such as PlatypusTech, one can engineer new types of sensing substrates for further improving the overall sensing performance of the SPR system.[19,34,36] As shown in Scheme 1, coating graphene layers or a layer of Au nanostructures (*e.g.*, nanoarrays, nanodots, nanogratings) on the SPR sensing film would substantially enhance the probing electric field at the sensing interface whereby leading to higher SPR sensitivities. Also, it is worth mentioning that the graphene-coated sensing substrate can effectively enhance the adsorption efficiency of target analytes that consist of carbon aromatic ring structures (*e.g.* DNA and RNA oligonucleotides) on the sensing surface through strong pi-stacking forces.[38,127] This unique feature from graphene-coated substrate will be important in the near future for designing label-free SPR sensing of DNA samples. In general, to employ graphene- or Au nanostructures-coated sensing substrate for enhanced sensing applications, one is required to theoretically optimize the number of graphene coating layers, the thickness of metallic thin film and the shape and size of Au nanostructures that are needed for achieving the best sensitivity in the SPR system by using analytical calculations based on Fresnel equations and numerical analysis through solving Maxwell equations based on the finite element method (FEM) or the finite-difference time-domain (FDTD) method, thereafter followed by experimental verification.[12,14] The last and the most important step for designing Au NPs-amplified SPR sensing is to optimize the size and shape of Au NPs that are employed as signal amplification tags in the experiments. It is known that the optical properties of Au NPs is closely related to their size and shape and one needs to select the Au NPs with extinction peaks that match well with the incident excitation wavelength in order to achieve the largest electric field enhancement between the Au NPs and the metallic sensing substrate, thus resulting in the highest SPR sensitivity for the target analyte sample.[16,57,91] For example, from our previous study,[12] we found that at a fixed separation distance of 5 nm between Au NPs and the sensing film, the electric field enhancement increases as the diameter of Au NP changes from 5 to 40 nm. However, it was observed that the electric field enhancement started to decrease when the diameter of Au NP further increased from 45 to 100 nm as indicated in Fig. 2. Based on our detailed analysis, the field enhancement possesses an optimal value when the diameter of Au NP is 40 nm and this means that the extinction peak of 40 nm Au NPs optically matched with the excitation wavelength and this also corresponds well with the prediction of Mie scattering theory on the 40 nm Au NPs that have a large absorption efficiency and small scattering efficiency.[128] However, it is reported that when the coupling distance between Au NPs and the sensing substrate is less than 3 nm, the extinction peak of Au NPs would have significantly redshifted with decreasing coupling distance and the values of their absorption- and scattering-coefficient would correspondingly change as well.[129] Thus, a detailed theoretical investigation of the electric field profile in a distance-dependent manner based on an estimated length of target analyte is needed for selecting the most suitable Au NPs for enhanced SPR sensing. The theoretical calculations can be performed by either using the finite element method (FEM) or the finite-difference time-domain (FDTD) method and such calculations are quite straightforward since many references and examples are available online for practicing. Once the optimized Au NPs is determined for the SPR sensing experiments, one can start to make or purchase the desired Au NPs for verifying the prediction of the calculation. Based on our experiences, a variation of 10 to 20% in the enhancement factor will be observed between theoretical estimation and experimental outcome and this variation is generally acceptable because theoretical calculations often assume ideal conditions in the simulation whereas experimental results will always relies on the actual parameters used during the study. We speculate that the variation will most likely originate from the precision of optical SPR sensing setup, the size distribution of the Au NPs, the overall thickness/roughness of the sensing film, and the mixture of buffers used in the experiments. It is also worth noting that the longitudinal extinction peaks of anisotropic Au NPs such as nanorods, nanoprisms and nanocubes are more flexible to be controlled than those of spherical Au NPs since their excitation peaks can be tuned from visible to infrared regions by tailoring the overall size and composition of the anisotropic Au NPs.[42,43,130] In addition, stronger field enhancements were recently reported at the edges of these anisotropic nanoparticles under SPR excitation conditions.[131,132] As such, these anisotropic Au NPs will certainly open up new avenues in the future rational design of anisotropic-based Au NPs-amplified SPR sensors for ultrasensitive detection of molecules with molecular mass below 8 kDa at concentration range between 1 aM and 1 pM. The guidelines mentioned here can be further extended and applied for designing other types of nanomaterial-based SPR sensors as long as all the computational parameters for the specific type of nanomaterial are correctly extracted or estimated from the literature.

3. Other nanomaterials-amplified SPR sensors

Although gold nanoparticles have been commonly used as SPR signal amplification tags or enhanced sensing surfaces, many research groups have started to explore and investigate other types of nanomaterials such as magnetic nanoparticles, carbon-based nanomaterials, silver nanoparticles, latex nanoparticles and liposome nanoparticles (see Table 2) for enhancing the SPR signals in the event of detecting interested ''hard-to-find'' analytes. In general, the enhancement principles of these nanomaterials in SPR sensing can be divided into three categories: (i) similar to Au NPs based SPR sensing method where LSPR of Au NPs are coupled with the surface plasmon wave excited on the sensing film, *e.g.*, silver nanoparticles; (ii) large surface mass loading that increases the sensitivity of the SPR sensing system, *e.g.*, latex nanoparticles, liposome nanoparticles and magnetic nanoparticles; and (iii) charge transfer from the nanomaterial surface to the metallic sensing

Table 2 Summary of other types of nanomaterials-amplified SPR sensors

Analyte	SPR sensor system	Enhancement strategy	Material scale	Limit of detection	Ref.
DNA and oligonucleotides					
Adenosine	Autolab SPR system	Colloidal Fe_3O_4 MNPs	32.82 nm	10 nM	22
hnRNP B1 mRNA	Custom-built (wavelength modulation)	Au nanoslits & colloidal Fe_3O_4 MNPs	6–10 nm	30 fM	154
Indicator for heart diseases					
Brain natriuretic peptide	Custom-built (angular reflectivity)	Colloidal Fe_2O_3 MNBs	50 nm	25 pg mL^{-1}	142
Allergens					
Ara h1	Custom-built fiber SPR (wavelength modulation)	Colloidal MNPs	19.0 ± 3.1 nm	0.09 μg mL^{-1}	143
Immunoassay					
CFP-10	Autolab SPR system	Colloidal NiO NPs	30 nm	0.1 ng mL^{-1}	155
hCG	Custom-built (angular reflectivity)	Colloidal latex NPs	238 nm	5 nM	20
βhCG	Custom-built (angular reflectivity)	Au grating & colloidal MNPs	220 nm	0.45 pM	156
Streptavidin	Custom-built (angular reflectivity)	Colloidal SPIONs	12 nm	125 nM	18
IFN-γ	IBIS	Colloidal liposome NPs	149.7–154.4 nm	100 pg mL^{-1}	21
Thrombin	Autolab SPR system	Colloidal Fe_3O_4 MNPs	10.46 nm	0.017 nM	24
Human GM–CSF	Biacore X	Colloidal CNTs	0.3–1.3 μm	0.1 ng mL^{-1}	149
Human erythropoietin	Biacore X	Colloidal CNTs	0.3–1.3 μm	0.1 ng mL^{-1}	149
Goat IgG	Custom-built SPRI	Colloidal silver NPs	10–40 nm	6.66 nM	152
Human IgG	Custom-built (wavelength modulation)	GO-coated Au thin film	mono- or bilayer	0.3 μg mL^{-1}	33
Mouse IgG	Custom-built (wavelength modulation)	GO sheets decorated with colloidal silver NPs	14 ± 3 nm	0.15 μg mL^{-1}	157
Organic molecules for calibration					
Glucose	Custom-built (phase detection)	Colloidal silver NPs	40 nm	6.3×10^{-8} RIU	151
Toxin in food					
Ochratoxin A	Biosuplar-3	Colloidal MNPs	200 nm	0.94 ng mL^{-1}	158

film surface that would induce a larger evanescent field enhancement thereby magnifying the SPR signals, *e.g.*, graphene and carbon nanotubes. In the following sections, we will introduce and discuss in detail about the designs and applications of enhanced SPR sensing systems integrated with these nanomaterials.

3.1 Magnetic nanoparticles

Magnetic nanoparticles (MNPs) have similar dimensions to that of the Au NPs and they have been used recently for SPR signal amplification studies. MNPs have a high surface area-to-volume ratio and therefore possess high surface energies for various chemical reactions. Also, they have versatile surface modification chemistry thereby allowing one to conveniently conjugate desired biomolecules on their surface. All these inherited features make them as ideal candidates for labeling and sensing of chemical and biological molecules. The bio-separation functions of MNPs for biological samples such as DNA, RNA, peptides, cells and virus have been extensively investigated in the past decade.[140,141] Also, the high molecular weight, high refractive index and cost-effective synthesis of MNPs have attracted great attention from the sensing community for applying them for enhanced SPR detection.

Teramura *et al.* demonstrated that the use of 50 nm magnetic nanobeads (MNBs) for enhanced SPR detection of picogram levels of brain natriuretic peptide (BNP) which is an important indicator for heart failure.[142] They first functionlized the Au sensing thin film with monolayers of carboxyl group-terminated alkanethiol (SH-(CH2)10-COOH, COOH-SAM) and then the primary monoclonal antibodies (BC203) were covalently immobilized onto the sensing surface and these antibodies were specific to BNP molecules. After injecting the solution of BNP followed by biotin-labeled secondary antibodies (KY-BNP-II) to the sensing substrate, a sandwich immunoassay was formed. The signal amplification was achieved by alternately accumulating the biotin-labeled anti-streptavidin antibody and streptavidin-conjugated nanobeads on the substrate surface to form several layers. The detection limit for BNP using this approach was determined to be 25 pg mL^{-1}. Pollet *et al.*[143] also designed a SPR enhancement strategy based on using secondary antibody-conjugated MNPs for selectively sensing the target analytes of peanut allergen – Ara h1 in chocolate candy bars. Their sensing scheme was based on a custom-built fiber SPR probe under wavelength modulation. The probe fiber was first coated with a thin layer of gold as the sensing surface and then modified with primary antibodies that were specific to Ara h1, while the super-paramagnetic nanoparticles with an average diameter of 19 nm were functionalized with polyclonal Ara h1 secondary antibodies by carbodiimide reactions. In this case, the primary antibody, Ara h1 and the secondary antibody labeled MNPs formed a sandwich immunoassay in the SPR system. Control experiments were also carried out for both label-free assay and secondary antibody sandwich assay in the absence of MNP labeling and the corresponding detection limits for the both assays were 9 μg mL^{-1} and 0.21 μg mL^{-1}, respectively, whereas a detection limit of 0.09 μg mL^{-1} was achieved for the MNPs-enhanced sandwich assay.

Zhou *et al.*[22] demonstrated the use of Fe_3O_4 MNPs as SPR amplification labels for detection of adenosine with a detection concentration range of 10–10^4 nM. The MNPs were synthesized by pyrolysis of iron carboxylate in an organic phase and later the particles were transferred to the aqueous phase by modifying their surface with hydrophilic moieties that possess carboxyl groups. MNPs with two different sizes (14.51 nm and 32.82 nm) were prepared for this study by tuning the ratio of FeO(OH) and oleic acid during the synthesis process. The MNPs with different concentrations (0.016–1.6 nM) were then bound to the thiol-modified SPR sensing films for studying their enhancement effect in the SPR system. It was found that the use of 32.82 nm MNPs resulted in a larger SPR signal change than that by employing 14.51 nm MNPs with same concentration. In addition, it was discovered that the SPR responses increased with the increase of MNPs concentration that resulted from the higher surface coverage of particles on the sensing substrate. The detection of adenosine in their experiment was based on indirect competitive inhibition assays (ICIAs). In the first step, 32.82 nm Fe_3O_4 MNPs at concentration of 1.6 nM were conjugated with antiadenosine aptamers, followed by the modification of the Au sensing film with the partial complementary antiadenosine aptamers. Next, the bioconjugated MNPs colloidal sample was flowed to the sensing surface thereby inducing a large SPR signal change that is due to the DNA hybridization process and high molecular weight and refractive index of MNPs. Lastly, upon the addition of target adenosine to the bioconjugated MNPs solution before injecting them to the sensing film, the structure of the aptamer conjugates on the surface of MNPs transformed into a tertiary structure which reduced the binding ability of MNPs to the sensing surface and this led to a significant decrease of the SPR signal change. Later, the same group[24] employed aptamer-conjugated Fe_3O_4 MNPs to form sandwich assays for enhanced SPR sensing of thrombin molecules. In this work, 1.5 nM Fe_3O_4 MNPs with an average diameter of 10.46 nm were conjugated with amino-modified anti-thrombin aptamers and the sensing surface of SPR system was functionalized with thiol-modified anti-thrombin aptamers. Next, solutions containing target thrombin were flowed into the sensing chip and followed by aptamer–Fe_3O_4 MNPs solution and this generated the formation of sandwich immunoassays where the target thrombin molecules were "captured" between the sensing film and MNPs. This enhancement scheme does not require any secondary antibodies that are commonly used in the conventional SPR sandwich immunoassay system. The detection limit of thrombin using this method was determined to be 0.017 nM and excellent selectivity was demonstrated when the control experimental results revealed that no responses were detected upon flowing BSA, human IgM and human IgE to the designed SPR system.

Lee *et al.* reported a SPR enhanced biosensing scheme using superparamagnetic iron oxide nanoparticles (SPIONs).[18] This scheme does not required initial receptor immobilization onto the sensing film. Streptavidin (SA) was used as the target analyte model in this enhanced SPR measurement. SPIONs were functionalized with biotin which enabled them to selectively bind to the SA. The enhanced sensing experiments were based on a custom-built angular SPR sensing system with a small piece of neodymium permanent magnet placed beneath the hemi-cylindrical prism. It was shown that under external magnetic fields, the aggregates of target SA and biotin–SPIONs were readily attracted to the sensing surface and subsequently induced a much larger SPR angle shift compared to the one without applying magnetic fields. The authors found that 12 nm SPIONs was the optimal diameter for the sensing applications and the detection limit for streptavidin (SA) using this approach was reported to be 125 nM.

3.2 Carbon-based nanomaterials

Functionalized carbon-based nanomaterials such as graphene[144,145] and carbon nanotubes[146,147] have recently been applied for enhanced SPR sensing applications. The use of graphene-coated Au sensing film for improving the SPR sensitivity was first proposed by Wu and co-workers in 2010.[19] They theoretically investigated the relationship between the number of graphene layers and SPR sensitivity to the refractive-index changes of sensing medium. An *N*-layer model (SF10 glass prism | Au thin film – 50 nm | graphene layers – $L \times 0.34$ nm | sensing medium) for transverse-magnetic wave was employed for the calculation of the total reflection under a well-known Kretschmann excitation configuration. It was demonstrated that through the angular measurement method, the SPR sensitivity increases with increasing number of graphene layers and a 25% enhancement factor was achieved when L equals 10. This enhancement effect was mainly due to the charge transfer from the surface of graphene to the surface of the Au thin film.[37] The charge transfer led to a stronger excited electric field on the surface of the Au thin film and made the sensing surface more sensitive towards the change in its surrounding medium.[12] The authors even proposed that this graphene-based SPR sensing method can be used to detect target analytes such as DNA and TNT because they can be easily adsorbed onto the sensing surface through a strong pi-stacking force between graphene and the aromatic ring structures-based target analytes.[127]

Later, Salihoglu *et al.*[30] fabricated the graphene-coated Au–Ag thin films and experimentally tested their enhanced SPR sensing performance (Fig. 9). The graphene was synthesized using the chemical vapor deposition (CVD) method and then transferred from the copper growth substrate into the metallic sensing film with the aid of PDMS stamps and an etching process using iron chloride solutions. It is worth noting that coating of graphene layers on the silver thin film can effectively prevent the oxidation of the silver sensing film used in the conventional SPR sensors.[34] From Salihoglu's angular SPR measurement results, the monolayer graphene-coated Au thin film showed a deeper dip at the resonance angle of the reflective spectrum when compared to the Au film without graphene coating. This indicated that a much stronger evanescent electric field at the graphene-coated sensing surface had been excited and thus would result in a higher SPR sensitivity. To further verify the detection and adsorption capabilities of the graphene-coated sensing surface, serum albumin proteins (BSAs) with different concentrations (40–500 nM) were employed as the target model and flowed onto the graphene-modified sensing film.

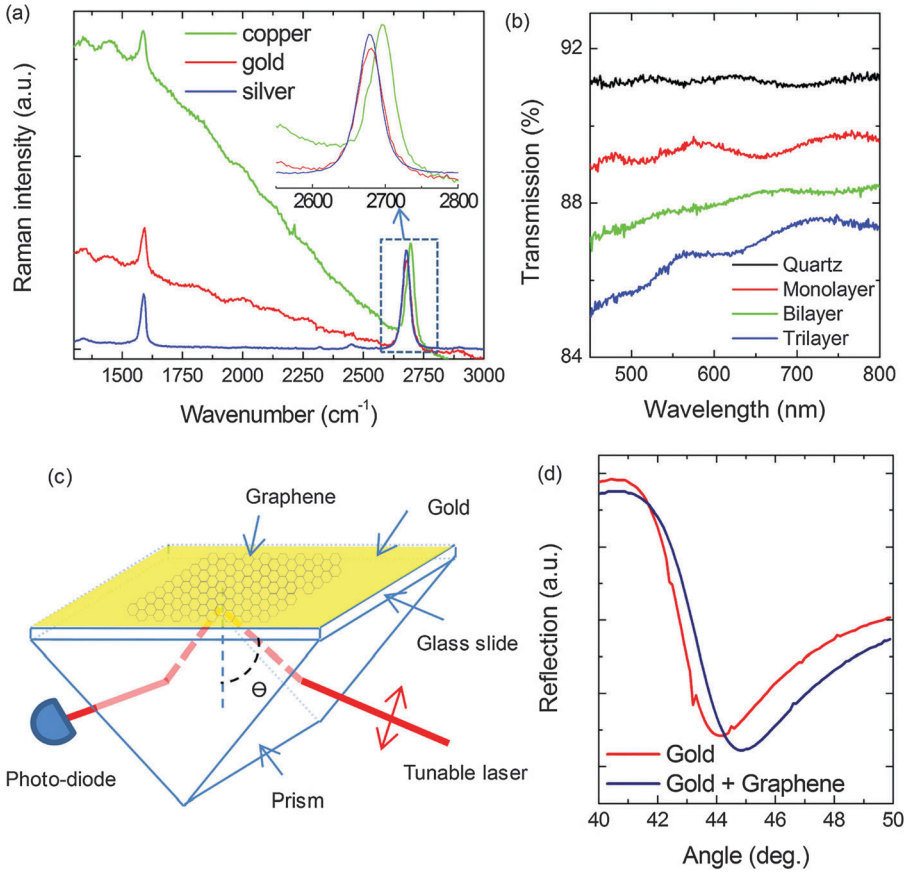

Fig. 9 (a) Raman spectra of as grown graphene on copper (green) and transfer printed graphene on silver (blue) and gold (red) surfaces. The intensity of the defect mode (D) is negligibly small. (b) Transmission spectra of multilayer graphene on transparent quartz substrates. Each layer has around 2% optical absorption. (c) Schematic representation of the Kretschmann configuration used to excite surface plasmon-polariton on the graphene–gold surface. (d) Surface plasmon resonance curves for the gold surface before (red) and after (blue) transfer printing graphene. The wavelength of the incident light is 632 nm. Reproduced from ref. 30 with permission of The American Institute of Physics.

From the SPR real-time monitoring, it was discovered that the association constant of BSA on the graphene-coated Au sensing film is around 2.4×10^{-5} M^{-1} s^{-1}. This value is roughly 3 times smaller than that of the anti-BSA modified capture Au sensing surface (7.4×10^{-5} M^{-1} s^{-1}). The SPR signal reached saturation after 20 min flow of BSA solution to the graphene-coated Au sensing film, and a very small dissociation constant was obtained during the wash process of the sensing film with 40 min flow of DI water. The small dissociate constant confirmed that BSA molecules were tightly bound to the graphene surface.

More recently, Zhang *et al.*[33] designed a graphene oxide (GO) sheet-coated Au thin film for enhanced SPR sensing applications. In this study, negatively charged GO was prepared using graphite powders based on a modified approach reported by Hummers and Offeman *et al.*[148] The GO was assembled onto the Au thin film by strong electrostatic forces. The thickness and surface roughness of the resulting GO sheets was characterized by atomic force microscopy (AFM). The AFM data revealed that the GO sheets were either monolayer or bilayer with high surface flatness. To investigate the SPR enhancement effect of this GO sheets-coated sensing film, human IgG was used and tested in the system as a target analyte. A custom-built SPR sensor based on wavelength modulations was used to monitor the antibody–antigen binding interactions. GO sheet-coated Au thin films were initially functionalized with goat anti-human IgG as a capture antibody. Subsequently, solutions containing target human IgG with different concentrations were flowed onto the sensing surface for evaluating the detection limit of the system. It was found that a minimum concentration of 0.3 μg mL^{-1} human IgG was needed to induce an observable SPR signal change of 0.22 nm. On the other hand, a 1.25 μg mL^{-1} human IgG was required to induce the SPR signal change when a conventional Au sensing film was applied in the SPR system. This demonstrated that the SPR detection limit of the GO sheets-coated Au thin film was 4 times more sensitive than that of the conventional Au sensing film.

Carbon nanotubes (CNTs) are different from the two-dimensional graphene layers which act more like MNPs as functionalized amplification tags for SPR detection since they have large surface area and molecular weight. Chung's group[149] reported the use of CNTs conjugation with secondary antibodies for enhanced SPR detection of human erythropoietin (EPO) and human granulocyte macrophage colony-stimulating factor (GM-CSF) molecules (Fig. 10). CNTs conjugating with

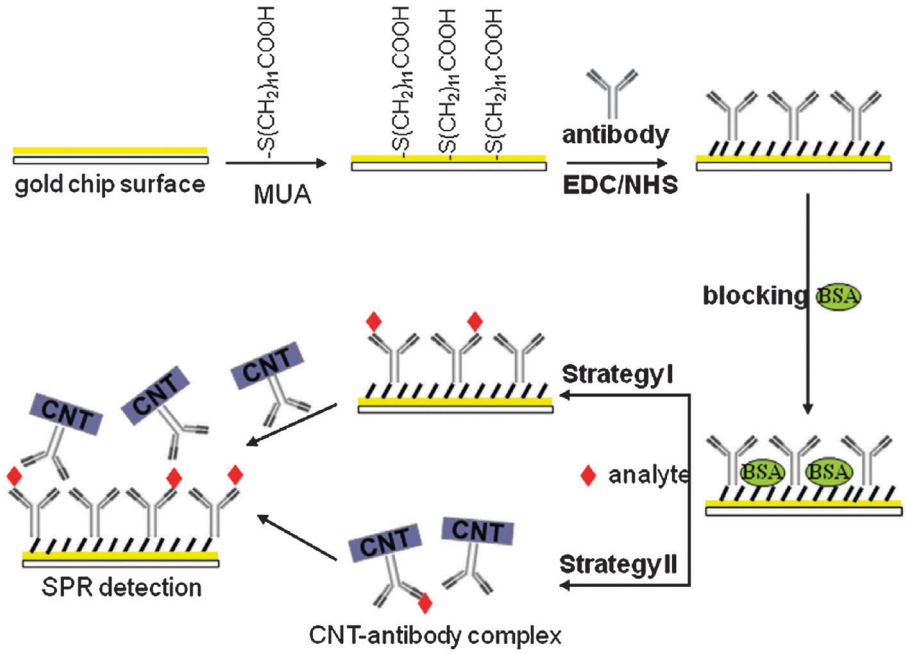

Fig. 10 Schematic diagram of SPR immunoassay to enhance sensitivity using the CNT–antibody complex. Reproduced from ref. 149 with permission of Elsevier.

secondary antibodies were obtained in two steps. First, the multiwalled CNTs were treated with H_2SO_4 : HNO_3 (3 : 1) solution for generating functional carboxylic groups on the surface of CNTs. Next, the functionalized CNTs with various sizes ranging from 0.3–1.3 μm were incubated with the secondary antibodies that were specific to EPO or GM-CSF, while the Au sensing films were respectively modified with the capture antibodies of EPO or GM-CSF. During the SPR sensing process, upon injecting the target antigens EPO or GM-CSF solution followed with the secondary antibodies labeled CNTs solution, a sandwich immunoassay detection scheme with target antigen analytes between the Au sensing film and CNTs was formed. The result showed that the SPR signals for both analytes were enhanced by more than 30 times when CNTs were used as the amplification tags in comparison to that in the label-free immunoassay detection scheme. Moreover, the detection sensitivity of this approach was determined to range from 0.1 to 1000 ng mL^{-1} for both analytes and a good linear logarithmic correlation was obtained between the SPR signal changes and the antigen concentrations.

3.3 Silver nanoparticles

Silver nanoparticles (Ag NPs)-coated SPR sensing films were found to have much better enhanced sensing performance when compared to Au NPs-coated ones because they have larger negative real part and smaller imaginary part in their dielectric constants.[132,150] Peng *et al.*[151] systematically studied the amplification effects of Ag NPs-coated films for enhanced SPR sensing of glucose. The Ag NPs-coated sensing film was fabricated based on a one-step thermal evaporation method. The authors investigated the SPR sensitivity of various Ag NPs-coated sensing films that were fabricated under different synthesis parameters. By controlling the synthesis parameters such as silver substrate temperature (50–150 °C), deposition thickness of the Ag NPs layer (1–10 nm) and the average size of Ag NPs (40–58 nm), different morphologies and surface roughness of Ag NPs-coated films were obtained. The highest SPR sensitivity of 6.3×10^{-8} RIU was obtained by using a 40 nm Ag NPs-coated sensing film in the glucose detection experiments. These experiments were performed by employing a custom-built phase interrogation SPR biosensor with an excitation wavelength of 632.8 nm. In addition to the above-mentioned thermal-evaporated Ag NPs, colloidal Ag NPs also demonstrated their capability as amplification tags for enhanced SPR sensing. Paul *et al.*[152] investigated the detection sensitivity of colloidal anti-IgG conjugated Ag NPs using a SPR microarray sensing instrument and found a 4-fold signal enhancement for 6.66 nM target goat IgG when compared to that of SPR measurements in the absence of Ag NPs. Here, Ag NPs with diameters ranging from 10 to 40 nm were prepared by the colloidal synthesis approach where tetrahydrofurans (THFs) are used as stabilizers and they were later functionalized with capture antibodies (anti-goat IgGs) for sensing use. From TEM analysis, the functionalization ratio between Ag NPs and the anti-goat IgG was estimated to be 1 : 5. The Au sensing film was pre-modified by 11-mercaptoundecanoic acid (MUA) solution. The rabbit anti-goat IgGs were later immobilized onto the MUA-Au sensing film and acted as capture molecules for detection of target goat IgG. The detection process firstly involved the injection of solutions containing target goat IgG with various concentrations (6.6 nM to 660 nM) into the anti-IgG modified sensing film and followed by flowing the Ag NPs–anti-IgG solution to the interface for signal amplification. The binding processes of target goat IgGs and rabbit anti-goat IgGs were monitored by the reflectivity change in percentage at an excitation wavelength of 552 nm and at a fixed incident angle of 46°. The authors

suggested that the detection limit of 6.6 nM for target goat IgG could be further improved by optimizing the incident angle parameter.

3.4 Latex nanoparticles

Latex nanoparticles were the first-generation nanomaterials used for enhanced SPR sensing. They were used back then for SPR sensing when the Au NPs enhanced SPR system was still in the early development stage. The signal enhancements of latex nanoparticles are solely based on their large size, surface area and molecular weight that lead to a large refractive-index change in the SPR sensing system. Also, latex particles are made from an amorphous polymer such as polystyrene and thus no coupling effect will occur between the particles and the surface plasmon waves on the sensing film. It was reported that the SPR amplification signal from latex nanoparticles is usually much lower than that using Au NPs formulation. Severs and Schasfoort[20] reported a SPR amplifcation stategy by using functionalized latex nanoparticles for detecting pregnancy hormone human chorionic gonadotropin (hCG). The authors have employed an inhibition detection format where the target hCG with different concentrations is conjugated with latex nanoparticles and subsequently mixtures of anti-hCG and target hCG-latex nanoparticle solutions are then flowed onto hCG-modified sensing films for evaluating the designed detection platform. In the reference sensing process, the target hCG-latex nanoparticle was absent in the mixture solution and thus the binding of anti-hCG with capture hCG on the Au sensing film resulted in a large a SPR signal change – 600 millidegrees. In the detection process, less anti-hCG bound to the sensing surface with increased concentration of target hCG-latex nanoparticle in the mixture solution and thus the SPR signal change dropped to a much lower level. The detection range of hCG can be manipulated by changing the concentration of anti-hCG in the mixture solution during the inhibition process. Using this method, it was found that the SPR enhancement factor was 30 when compared to the experiments without using latex nanoparticles and a detect limit of 5 nM was achieved for hCG.

3.5 Liposome nanoparticles

Liposome nanoparticles are artificial phospholipid vesicles with diameters larger than 100 nm and they are known to be effective carriers for drug delivery.[153] Similar to latex nanoparticles, the binding of liposome nanoparticles to the SPR sensing surface can also induce large perturbation to the excited evanescent field and lead to a large signal change. This is caused by the large size and high refractive index of the particles. Wink *et al.*[21] demonstrated the use of liposome nanoparticles ($\sim$150 nm) as amplification tags in SPR sensing system for detecting interferon-γ (IFN-γ), a cytokine with a molecular weight of 16 kDa. They specifically designed a liposome sandwich immunosorbent assay (LISA) to perform their experiments. At the beginning, the SPR sensing surface was modified with capture antibodies (MD-2) and then post-coated with casein. Then, target antigen–IFN-γ solution was injected into the sensing surface followed by solution of secondary biotinylated antibodies (MD-1) that were specific to another epitope of the target IFN-γ. Next, avidin and biotinylated liposomes were injected in order in sequence to the SPR sensing film and liposomes nanoparticles were bound to the avidin–MD-1 conjugates to create a significant SPR signal change. The detection limit of this LISA approach was determined to be 100 pg mL^{-1} for IFN-γ molecules. This result shows that the obtained sensitivity is four orders of magnitude more sensitive than that of the one without using liposome nanoparticles as amplification labels.

4. Summary and future outlook

Detection of biological and chemical molecules with a small molecular weight less than 8 kDa at extremely dilute conditions is essential for applications ranging from early cancer diagnosis to security monitoring. However, it is challenging for many conventional sensors to achieve this goal especially for some specific analytes like cancer biomarkers in human blood serum. During the past two decades, SPR sensors have served as an effective tool for real-time detecting of molecular interactions at the sensing substrate. Recently, with the rapid growth of nanotechnology, many enhanced SPR sensing strategies incorporated with functional nanomaterials have been exploited for the ultrasensitive detection of different biological and chemical analytes. Gold nanoparticles are the most widely used nanomaterials in ultrasensitive SPR sensing of analytes because they are easy to be prepared and functionalized with various chemical and biological molecules. As a result, many of them are currently available for sale in different chemical companies. For instance, dispersions of spherical gold nanoparticles, nanorods, nanowires, nanocomposites (with Pt, Pd and trimetallic coating) terminated with functional groups (*e.g.*, amine, biotin, carboxyl, maleimide, methyl, neutravidin and streptavidin) or conjugated with secondary antibodies (*e.g.*, protein A/G, goat anti-human IgA/IgG/IgM, goat anti-mouse IgG and goat anti-rabbit IgG) with a shelf-life of up to 18 months can be purchased from Nanopartz Inc. and Sigma-Aldrich. The availability and long shelf-life of these products will allow one to select and design the most appropriate Au NPs formulation for long-term and real-time SPR detection. In general, gold nanoparticles can be either used as label-free enhanced sensing substrate or functional amplification tags in the SPR sensing experiments because they have rich surface modification chemistries and their LSPR is able to couple with the surface plasmon waves on the PSPR sensing film for enhancing the SPR signals. Label-free enhanced sensing substrate based on gold nanoparticles (*e.g.*, Au nanoarrays-coated sensing film) are more convenient and time-saving for sensing applications in comparison of using them as amplification nanotags where a sandwich immunoassay pattern is needed during the sensing process. However, the fabrication of label-free enhanced sensing substrate based on gold nanoparticles is expensive and tedious processing steps are needed to generate useable gold nanoparticles-based sensing substrates. It is worth mentioning that other novel nanostructures such as gold nanocubes and nanoprisms are currently under investigation by many research groups and they want to use them as functional amplification tags for ultrasensitive SPR

sensing applications.[57] The enhancement principle for SPR sensors based on silver nanoparticles is similar to that using gold nanoparticles. Silver nanoparticles even have better coupling effect when immobilizing them onto the sensing film of PSPR sensors and thus result in higher SPR sensitivity, but the chemical inertness and long-term stability of silver nanoparticles are difficult to realize. Choi *et al.*[159] recently reported the fabrication of a label-free sensing film coated with closely-spaced silver nanodome arrays on SiO_2/plastic sheets. The sensing film can be prepared at a very low cost and allows one to dispose it after single-use. This engineering approach will effectively overcome the challenges of oxidization and long-term repeatability for employing silver nanoparticles-enhanced SPR sensors. Thus, it is crucial for one to understand and select the best enhanced SPR sensing scheme for its own specific applications. In the near future, we foresee that SPR sensors with label-free enhanced sensing substrate based on various gold–silver nanostructures (*e.g.* slits, gratings and dot- or rod-arrays) will play a key role in biomedical and environmental sensing applications since they have the potential to be miniaturized as a portable device for on-site monitoring of samples ranging from infected blood to contaminated water samples.

Magnetic nanoparticles and carbon-based nanomaterials (*e.g.*, graphene and carbon nanotubes) have emerged as a new class of building blocks for engineering enhanced SPR sensors. These nanomaterials can be prepared at a low production cost and more importantly they can be easily hybridized with metallic thin films or metallic nanoparticles thereby allowing them to detect desired molecules under SPR sensing schemes such as the sandwich detection scheme and indirect competitive inhibition detection scheme.[154] One unique feature of using magnetic nanoparticles (MNPs) as SPR amplification tags when compared to other nanomaterials is their bioseparation function for selective separation and detecting target analyte samples in a complex physiological matrix with high viscosity such as blood plasma. For example, the MNPs can be functionalized with capture molecules of the target analyte and used to separate the target analyte from the physiological sample solution by an external magnetic field for reducing the nonspecific binding events of target analyte during the SPR sensing process. The large-scale preparation of high-quality graphene sheets using the CVD method has been demonstrated by Ruoff's group.[160] The graphene layer-coated Au or Ag thin films are promising sensing substrates to be used in the next generation enhanced SPR sensors since they are able to generate strong enhancement effects during the coupling process between target analytes and the sensing surface. Here, we want to point out that the majority of reported graphene-coated gold sensing films were fabricated by self-assembly of monolayer or bilayer graphene oxide sheets on a positively charged metallic thin film. In general, the graphene oxide is prepared in a suspension form before coating it onto the sensing film as sheet/s that are terminated with negatively charged groups such as hydroxyl groups. Since the optical and electronic properties of graphene oxide sheets are very different from those of pristine graphene sheets synthesized using exfoliation and chemical vapor deposition (CVD) methods, the enhanced SPR effect of graphene oxide-modified sensing film will thus be compromised. This is mainly due to the conductivity and dielectric properties of graphene oxide.[161] As the conductivity and dielectric constant of graphene oxide are lower than that of the pristine graphene, fewer electrons will transfer from the surface of graphene oxide to the surface of metallic thin film thereby leading to a much smaller electric field enhancement at the sensing film surface. Thus, the SPR enhancement factor will be much lower for sensing films coated with graphene oxide sheets in comparison to those functionalized with pristine graphene sheets. Our group has recently systematically investigated gold nanofilms modified with different layers of CVD graphene sheets as sensing films for improving SPR sensitivity to the sub-femtomolar level. Basically, we fabricated the pristine monolayer graphene coated gold nanofilm and employed the sensing film for sensing ssDNA molecules with a molecular weight of 7.3 kDa. A detection limit of 0.1 fM for the 24 mer ssDNA molecules was achieved by using the prepared sensing film and a custom-built phase-sensitive PSPR sensor. Our system will serve as a useful platform for providing a set of guidelines for engineering the next generation of SPR sensors for clinical and biosciences needs.

Latex and liposome nanoparticles might not be the most popular enhanced nanomaterials to be used for SPR sensing as they can only work as the amplification tags in terms of their high refractive index that results from their large particle size,[153] but one can use them as a powerful platform to create hybrid colloidal nanoparticles as "effective" amplification tags that will be very useful for ultrasensitive SPR detection. For example, hybrid colloidal particles such as Au NPs-coated polystyrene microspheres,[162] Ag NPs-coated polystyrene beads,[163] and Au NPs-loaded phosphatidyl-choline (PC) vesicles[164] have recently been reported and they can be easily incorporated with various SPR sensing strategies for screening desired biomolecules such as pathogens. More importantly, we can foresee that these hybrid nanoparticles can be functionalized with targeting molecules for further improving the sensitivity of PSPR sensors. Nevertheless, we want to emphasize that the preparation of these nanoparticles is not straightforward and a skillful nanotechnologist is required to synthesize the optimized particles formulation for SPR detection since there are many different synthesis protocols available in the literature.

We wish to highlight that all the nanomaterials-based enhanced SPR sensing strategies discussed here are not solely for achieving highest sensitivity detection but they also have the abilities to perform multiplex sensing of different target analytes through one screening of samples. This can be realized by optimizing the morphologies of the sensing substrate, types of the amplification tags used, selective immobilization of receptor molecules on the arrays of the sensing substrate, and surface functionalization of the amplification tags with specific capture-molecules. Moreover, although the enhanced SPR sensing based on nanomaterials are commonly tested using standard and well-known target analytes like human IgA/IgG/IgM, it is also applicable to other important biological/medicinal samples for clinical diagnostics such as amyloid-derived diffusible ligands (ADDLs) – Alzheimer's disease (AD) peptide biomarkers[165,166] and human dihydrofolate

reductase (hDHFR) – protein indicator for malignancies.[167,168] Also, in the lists of Tables 1 and 2, one can clearly observe that many of the reported nanomaterial enhanced SPR sensing experiments are employing commercially available SPR instruments such as the Autolab SPR system, Biacore Q/X/2000/3000, Biosuplar-2/3, IBIS, NanoSPR-321 and SPReeta system in their study and thus we envision that nanomaterial-amplified SPR sensors will be quickly adopted and integrated into the commercial SPR instruments in the near future. Such newly engineered portable nano-SPR instruments will serve as powerful platforms for advanced sensing of molecules under harsh and extreme conditions.

References

1 P. N. Prasad, *Introduction to Biophotonics*, Wiley-Interscience, New York, 2003.
2 J. Homola, S. S. Yee and G. Gauglitz, *Sens. Actuators, B*, 1999, **54**, 3–15.
3 X. D. Hoa, A. G. Kirk and M. Tabrizian, *Biosens. Bioelectron.*, 2007, **23**, 151–160.
4 A. Shalabney and I. Abdulhalim, *Laser Photonics Rev.*, 2011, **5**, 571–606.
5 E. E. Bedford, J. Spadavecchia, C. M. Pradier and F. X. Gu, *Macromol. Biosci.*, 2012, **12**, 724–739.
6 C. Situ, J. Buijs, M. H. Mooney and C. T. Elliott, *Trac, Trends Anal. Chem.*, 2010, **29**, 1305–1315.
7 S. Szunerits, N. Maalouli, E. Wijaya, J. P. Vilcot and R. Boukherroub, *Anal. Bioanal. Chem.*, 2013, **405**, 1435–1443.
8 H. Raether, *Surface plasmons on smooth and rough surfaces and on gratings*, Springer-Verlag, Berlin, 1988.
9 H. P. Ho and W. W. Lam, *Sens. Actuators, B*, 2003, **96**, 554–559.
10 H. P. Ho, W. C. Law, S. Y. Wu, X. H. Liu, S. P. Wong, C. L. Lin and S. K. Kong, *Sens. Actuators, B*, 2006, **114**, 80–84.
11 M. E. Stewart, C. R. Anderton, L. B. Thompson, J. Maria, S. K. Gray, J. A. Rogers and R. G. Nuzzo, *Chem. Rev.*, 2008, **108**, 494–521.
12 S. W. Zeng, X. Yu, W.-C. Law, Y. Zhang, R. Hu, X.-Q. Dinh, H.-P. Ho and K.-T. Yong, *Sens. Actuators, B*, 2013, **176**, 1128–1133.
13 S. W. Zeng, K.-T. Yong, I. Roy, X.-Q. Dinh, X. Yu and F. Luan, *Plasmonics*, 2011, **6**, 491–506.
14 A. V. Kabashin, P. Evans, S. Pastkovsky, W. Hendren, G. A. Wurtz, R. Atkinson, R. Pollard, V. A. Podolskiy and A. V. Zayats, *Nat. Mater.*, 2009, **8**, 867–871.
15 W. C. Law, P. Markowicz, K. T. Yong, I. Roy, A. Baev, S. Patskovsky, A. V. Kabashin, H. P. Ho and P. N. Prasad, *Biosens. Bioelectron.*, 2007, **23**, 627–632.
16 W. C. Law, K. T. Yong, A. Baev and P. N. Prasad, *ACS Nano*, 2011, **5**, 4858–4864.
17 W. C. Law, K. T. Yong, A. Baev, R. Hu and P. N. Prasad, *Opt. Express*, 2009, **17**, 19041–19046.
18 K. S. Lee, M. Lee, K. M. Byun and I. S. Lee, *J. Mater. Chem.*, 2011, **21**, 5156–5162.
19 L. Wu, H. S. Chu, W. S. Koh and E. P. Li, *Opt. Express*, 2010, **18**, 14395–14400.
20 A. H. Severs and R. B. M. Schasfoort, *Biosens. Bioelectron.*, 1993, **8**, 365–370.
21 T. Wink, S. J. van Zuilen, A. Bult and W. P. van Bennekom, *Anal. Chem.*, 1998, **70**, 827–832.
22 J. L. Wang, A. Munir, Z. Z. Zhu and H. S. Zhou, *Anal. Chem.*, 2010, **82**, 6782–6789.
23 J. A. Wang, Y. Sun, L. Y. Wang, X. N. Zhu, H. Q. Zhang and D. Q. Song, *Colloids Surf., B*, 2010, **81**, 600–606.
24 J. L. Wang, Z. Z. Zhu, A. Munir and H. S. Zhou, *Talanta*, 2011, **84**, 783–788.
25 L. Y. Wang, Y. Sun, J. Wang, J. A. Wang, A. M. Yu, H. Q. Zhang and D. Q. Song, *Colloids Surf., B*, 2011, **84**, 484–490.
26 F. Yu, B. Persson, S. Lofas and W. Knoll, *J. Am. Chem. Soc.*, 2004, **126**, 8902–8903.
27 X. D. Fan, I. M. White, S. I. Shopova, H. Y. Zhu, J. D. Suter and Y. Z. Sun, *Anal. Chim. Acta*, 2008, **620**, 8–26.
28 N. Granqvist, A. Hanning, L. Eng, J. Tuppurainen and T. Viitala, *Sensors*, 2013, **13**, 15348–15363.
29 L. P. Xia, S. Y. Yin, H. T. Gao, Q. L. Deng and C. L. Du, *Plasmonics*, 2011, **6**, 245–250.
30 O. Salihoglu, S. Balci and C. Kocabas, *Appl. Phys. Lett.*, 2012, **100**, 213110.
31 L. Wang, C. Z. Zhu, L. Han, L. H. Jin, M. Zhou and S. J. Dong, *Chem. Commun.*, 2011, **47**, 7794–7796.
32 A. N. Grigorenko, M. Polini and K. S. Novoselov, *Nat. Photonics*, 2012, **6**, 749–758.
33 H. Zhang, Y. Sun, S. Gao, J. Zhang, H. Zhang and D. Song, *Small*, 2013, **9**, 2537–2540.
34 S. H. Choi, Y. L. Kim and K. M. Byun, *Opt. Express*, 2011, **19**, 458–466.
35 Y. Mao, Y. Bao, W. Wang, Z. Li, F. Li and L. Niu, *Talanta*, 2011, **85**, 2106–2112.
36 V. V. Singh, G. Gupta, A. Batra, A. K. Nigam, M. Boopathi, P. K. Gutch, B. K. Tripathi, A. Srivastava, M. Samuel, G. S. Agarwal, B. Singh and R. Vijayaraghavan, *Adv. Funct. Mater.*, 2012, **22**, 2352–2362.
37 G. Giovannetti, P. A. Khomyakov, G. Brocks, V. M. Karpan, J. van den Brink and P. J. Kelly, *Phys. Rev. Lett.*, 2008, **101**, 026803.
38 S. Akca, A. Foroughi, D. Frochtzwajg and H. W. C. Postma, *PLoS One*, 2011, **6**, e18442.
39 C. M. Cobley, J. Y. Chen, E. C. Cho, L. V. Wang and Y. N. Xia, *Chem. Soc. Rev.*, 2011, **40**, 44–56.
40 X. Hong and E. A. H. Hall, *Analyst*, 2012, **137**, 4712–4719.
41 K. Saha, S. S. Agasti, C. Kim, X. N. Li and V. M. Rotello, *Chem. Rev.*, 2012, **112**, 2739–2779.
42 H. Ding, K. T. Yong, I. Roy, H. E. Pudavar, W. C. Law, E. J. Bergey and P. N. Prasad, *J. Phys. Chem. C*, 2007, **111**, 12552–12557.
43 J. Zhu, K. T. Yong, I. Roy, R. Hu, H. Ding, L. L. Zhao, M. T. Swihart, G. S. He, Y. P. Cui and P. N. Prasad, *Nanotechnology*, 2010, **21**, 285106.
44 M. S. Golden, A. C. Bjonnes and R. M. Georgiadis, *J. Phys. Chem. C*, 2010, **114**, 8837–8843.

45 M. Hu, J. Y. Chen, Z. Y. Li, L. Au, G. V. Hartland, X. D. Li, M. Marquez and Y. N. Xia, *Chem. Soc. Rev.*, 2006, **35**, 1084–1094.
46 P. X. Zhao, N. Li and D. Astruc, *Coord. Chem. Rev.*, 2013, **257**, 638–665.
47 J. Turkevich, P. C. Stevenson and J. Hillier, *Discuss. Faraday Soc.*, 1951, **11**, 55–75.
48 J. Kimling, M. Maier, B. Okenve, V. Kotaidis, H. Ballot and A. Plech, *J. Phys. Chem. B*, 2006, **110**, 15700–15707.
49 S. Zeng, Y. Liang, H. Lu, L. Wang, X.-Q. Dinh, X. Yu, H.-P. Ho, X. Hu and K.-T. Yong, *Mater. Lett.*, 2012, **67**, 74–77.
50 B. Nikoobakht and M. A. El-Sayed, *Chem. Mater.*, 2003, **15**, 1957–1962.
51 X. C. Ye, L. H. Jin, H. Caglayan, J. Chen, G. Z. Xing, C. Zheng, D. N. Vicky, Y. J. Kang, N. Engheta, C. R. Kagan and C. B. Murray, *ACS Nano*, 2012, **6**, 2804–2817.
52 L. He, M. D. Musick, S. R. Nicewarner, F. G. Salinas, S. J. Benkovic, M. J. Natan and C. D. Keating, *J. Am. Chem. Soc.*, 2000, **122**, 9071–9077.
53 J. S. Mitchell, Y. Q. Wu, C. J. Cook and L. Main, *Anal. Biochem.*, 2005, **343**, 125–135.
54 J. S. Mitchell and T. E. Lowe, *Biosens. Bioelectron.*, 2009, **24**, 2177–2183.
55 D. J. Lin, J. Wu, M. Wang, F. Yan and H. X. Ju, *Anal. Chem.*, 2012, **84**, 3662–3668.
56 C. P. Chak, L. H. Chau, S. Y. Wu, H. P. Ho, W. J. Li, P. M. Mendes and K. C. F. Leung, *J. Mater. Chem.*, 2011, **21**, 8317–8323.
57 M. J. Kwon, J. Lee, A. W. Wark and H. J. Lee, *Anal. Chem.*, 2012, **84**, 1702–1707.
58 L. A. Lyon, M. D. Musick and M. J. Natan, *Anal. Chem.*, 1998, **70**, 5177–5183.
59 L. A. Lyon, M. D. Musick, P. C. Smith, B. D. Reiss, D. J. Pena and M. J. Natan, *Sens. Actuators, B*, 1999, **54**, 118–124.
60 L. A. Lyon, D. J. Pena and M. J. Natan, *J. Phys. Chem. B*, 1999, **103**, 5826–5831.
61 L. He, E. A. Smith, M. J. Natan and C. D. Keating, *J. Phys. Chem. B*, 2004, **108**, 10973–10980.
62 R. S. Moirangthem, Y. C. Chang and P. K. Wei, *Opt. Lett.*, 2011, **36**, 775–777.
63 J. Homola, *Chem. Rev.*, 2008, **108**, 462–493.
64 H. Sipova and J. Homola, *Anal. Chim. Acta*, 2013, **773**, 9–23.
65 W. Yuan, H. P. Ho, R. K. Y. Lee and S. K. Kong, *Appl. Opt.*, 2009, **48**, 4329–4337.
66 K. A. Peterlinz, R. M. Georgiadis, T. M. Herne and M. J. Tarlov, *J. Am. Chem. Soc.*, 1997, **119**, 3401–3402.
67 T. T. Goodrich, H. J. Lee and R. M. Corn, *J. Am. Chem. Soc.*, 2004, **126**, 4086–4087.
68 Y. Liu and W. D. Wilson, *Drug-DNA Interaction Protocols*, Humana Press, New York, 2010.
69 M. Hayashida, A. Yamaguchi and H. Misawa, *Jpn. J. Appl. Phys., Part 2*, 2005, **44**, L1544–L1546.
70 S. Moon, D. J. Kim, K. Kim, D. Kim, H. Lee, K. Lee and S. Haam, *Appl. Opt.*, 2010, **49**, 484–491.
71 X. Yao, X. Li, F. Toledo, C. Zurita-Lopez, M. Gutova, J. Momand and F. M. Zhou, *Anal. Biochem.*, 2006, **354**, 220–228.
72 F. Y. Song, F. M. Zhou, J. Wang, N. J. Tao, J. Q. Lin, R. L. Vellanoweth, Y. Morquecho and J. Wheeler-Laidman, *Nucleic Acids Res.*, 2002, **30**, e72.
73 J. L. Wang and H. S. Zhou, *Anal. Chem.*, 2008, **80**, 7174–7178.
74 J. L. Wang, A. Munir and H. S. Zhou, *Talanta*, 2009, **79**, 72–76.
75 X. Ni, M. Castanares, A. Mukherjee and S. E. Lupold, *Curr. Med. Chem.*, 2011, **18**, 4206–4214.
76 G. Z. Zhu, M. Ye, M. J. Donovan, E. Q. Song, Z. L. Zhao and W. H. Tan, *Chem. Commun.*, 2012, **48**, 10472–10480.
77 S. Fang, H. J. Lee, A. W. Wark and R. M. Corn, *J. Am. Chem. Soc.*, 2006, **128**, 14044–14046.
78 J. R. Horton, M. Y. Mabuchi, D. Cohen-Karni, X. Zhang, R. M. Griggs, M. Samaranayake, R. J. Roberts, Y. Zheng and X. D. Cheng, *Nucleic Acids Res.*, 2012, **40**, 9763–9773.
79 P. Kielkowski, N. L. Brock, J. S. Dickschat and M. Hocek, *ChemBioChem*, 2013, **14**, 801–804.
80 Q. F. Luan, K. B. Zhou, H. N. Tan, D. Yang and X. Yao, *Biosens. Bioelectron.*, 2011, **26**, 2473–2477.
81 N. Nagase, K. Terao, N. Miyanishi, K. Tamai, N. Uchiyama, T. Suzuki, H. Takao, F. Shimokawa and F. Oohira, *Analyst*, 2012, **137**, 5034–5040.
82 C. H. Chen, X. Q. Zhang, C. W. Lo, P. F. Liu, Y. T. Liu, R. L. Gallo, M. F. Hsieh, R. T. Schooley and C. M. Huang, *Proteomics*, 2010, **10**, 2396–2401.
83 J. Yang, Y. C. Song, T. S. Song, X. Y. Hu, Y. M. Guo, Z. F. Li, C. X. Dang and C. Huang, *J. Clin. Lab. Anal.*, 2012, **26**, 148–154.
84 J. H. Gu, H. Lü, Y. W. Chen, L. Y. Liu, P. Wang, J. M. Ma and Z. H. Lu, *Supramol. Sci.*, 1998, **5**, 695–698.
85 J. L. Wang, A. Munir, Z. H. Li and H. S. Zhou, *Biosens. Bioelectron.*, 2009, **25**, 124–129.
86 K. Maehashi, T. Katsura, K. Kerman, Y. Takamura, K. Matsumoto and E. Tamiya, *Anal. Chem.*, 2007, **79**, 782–787.
87 S. Ko, T. J. Park, H. S. Kim, J. H. Kim and Y. J. Cho, *Biosens. Bioelectron.*, 2009, **24**, 2592–2597.
88 C. Cao and S. J. Sim, *Biosens. Bioelectron.*, 2007, **22**, 1874–1880.
89 Y. Liu and Q. Cheng, *Anal. Chem.*, 2012, **84**, 3179–3186.
90 P. Hao, Y. H. Wu and F. J. Li, *Appl. Opt.*, 2011, **50**, 5555–5558.
91 V. G. Kravets, F. Schedin, R. Jalil, L. Britnell, R. V. Gorbachev, D. Ansell, B. Thackray, K. S. Novoselov, A. K. Geim, A. V. Kabashin and A. N. Grigorenko, *Nat. Mater.*, 2013, **12**, 304–309.
92 M. Riskin, Y. Ben-Amram, R. Tel-Vered, V. Chegel, J. Almog and I. Willner, *Anal. Chem.*, 2011, **83**, 3082–3088.
93 M. E. Roberts, M. C. LeMieux and Z. N. Bao, *ACS Nano*, 2009, **3**, 3287–3293.
94 K. K. Kartha, S. S. Babu, S. Srinivasan and A. Ajayaghosh, *J. Am. Chem. Soc.*, 2012, **134**, 4834–4841.
95 M. Riskin, R. Tel-Vered, O. Lioubashevski and I. Willner, *J. Am. Chem. Soc.*, 2009, **131**, 7368–7378.
96 M. Frasconi, R. Tel-Vered, M. Riskin and I. Willner, *Anal. Chem.*, 2010, **82**, 2512–2519.
97 Y. Ben-Amram, R. Tel-Vered, M. Riskin, Z. G. Wang and I. Willner, *Chem. Sci.*, 2012, **3**, 162–167.

98 X. Huang, H. Y. Tu, D. H. Zhu, D. Du and A. D. Zhang, *Talanta*, 2009, **78**, 1036–1042.
99 A. E. Urusov, S. N. Kostenko, P. G. Sveshnikov, A. V. Zherdev and B. B. Dzantiev, *Sens. Actuators, B*, 2011, **156**, 343–349.
100 K. V. Gobi, H. Iwasaka and N. Miura, *Biosens. Bioelectron.*, 2007, **22**, 1382–1389.
101 J. Trevino, A. Calle, J. M. Rodriguez-Frade, M. Mellado and L. M. Lechuga, *Clin. Chim. Acta*, 2009, **403**, 56–62.
102 A. Ramanaviciene, N. German, A. Kausaite-Minkstimiene, J. Voronovic, J. Kirlyte and A. Ramanavicius, *Biosens. Bioelectron.*, 2012, **36**, 48–55.
103 R. I. G. Holt and P. H. Sonksen, *Br. J. Pharmacol.*, 2008, **154**, 542–556.
104 P. E. Sottas, N. Robinson, O. Rabin and M. Saugy, *Clin. Chem.*, 2011, **57**, 969–976.
105 S. Korsatko, K. Glettler, K. J. Olsen, A. Wutte, G. Bock, G. Koehler, J. K. Mader, B. Semlitsch and T. R. Pieber, *Diabetes, Obes. Metab.*, 2013, **15**, 241–245.
106 M. Y. Xu, X. L. Luo and J. J. Davis, *Biosens. Bioelectron.*, 2013, **39**, 21–25.
107 M. Frasconi, C. Tortolini, F. Botre and F. Mazzei, *Anal. Chem.*, 2010, **82**, 7335–7342.
108 P. V. Lishko, I. L. Botchkina and Y. Kirichok, *Nature*, 2011, **471**, 387–391.
109 L. Vignozzi, A. Morelli, E. Sarchielli, P. Comeglio, S. Filippi, I. Cellai, E. Maneschi, S. Serni, M. Gacci, M. Carini, M. P. Piccinni, F. Saad, L. Adorini, G. B. Vannelli and M. Maggi, *J. Endocrinol.*, 2012, **212**, 71–84.
110 E. H. Gillis, I. Traynor, J. P. Gosling and M. Kane, *J. AOAC Int.*, 2006, **89**, 838–842.
111 G. Corona, M. Monami, G. Rastrelli, A. Aversa, Y. Tishova, F. Saad, A. Lenzi, G. Forti, E. Mannucci and M. Maggi, *J. Sex. Med.*, 2011, **8**, 272–283.
112 J. Mitchell, *Sensors*, 2010, **10**, 7323–7346.
113 C. C. Huang, Y. R. Lien, H. F. Chen, M. J. Chen, C. J. Shieh, Y. L. Yao, C. H. Chang, S. U. Chen and Y. S. Yang, *Hum. Reprod.*, 2012, **27**, 2036–2045.
114 J. Yuan, R. Oliver, J. Li, J. Lee, M. Aguilar and Y. Wu, *Biosens. Bioelectron.*, 2007, **23**, 144–148.
115 M. Zayats, S. P. Pogorelova, A. B. Kharitonov, O. Lioubashevski, E. Katz and I. Willner, *Chem.–Eur. J.*, 2003, **9**, 6108–6114.
116 S. Y. Gao, N. Koshizaki, H. Tokuhisa, E. Koyama, T. Sasaki, J. K. Kim, J. Ryu, D. S. Kim and Y. Shimizu, *Adv. Funct. Mater.*, 2010, **20**, 78–86.
117 M. Mitsushio, K. Miyashita and M. Higo, *Sens. Actuators, A*, 2006, **125**, 296–303.
118 S. Link, Z. L. Wang and M. A. El-Sayed, *J. Phys. Chem. B*, 1999, **103**, 3529–3533.
119 C. B. Gao, Z. D. Lu, Y. Liu, Q. Zhang, M. F. Chi, Q. Cheng and Y. D. Yin, *Angew. Chem., Int. Ed.*, 2012, **51**, 5629–5633.
120 J. Wang, D. Q. Song, L. Y. Wang, H. Zhang, H. Q. Zhang and Y. Sun, *Sens. Actuators, B*, 2011, **157**, 547–553.
121 L. Y. Wang, Y. Sun, J. A. Wang, J. Wang, A. M. Yu, H. Q. Zhang and D. Q. Song, *J. Colloid Interface Sci.*, 2010, **351**, 392–397.
122 X. Wang, X. G. Kong, Y. Yu and H. Zhang, *J. Phys. Chem. C*, 2007, **111**, 3836–3841.
123 Y. C. Wang, K. C. L. Black, H. Luehmann, W. Y. Li, Y. Zhang, X. Cai, D. H. Wan, S. Y. Liu, M. Li, P. Kim, Z. Y. Li, L. H. V. Wang, Y. J. Liu and Y. A. Xia, *ACS Nano*, 2013, **7**, 2068–2077.
124 B. Pelaz, V. Grazu, A. Ibarra, C. Magen, P. del Pino and J. M. de la Fuente, *Langmuir*, 2012, **28**, 8965–8970.
125 P. J. Wang, M. Y. Liu, G. L. Gao, S. P. Zhang, H. L. Shi, Z. P. Li, L. S. Zhang and Y. Fang, *J. Mater. Chem.*, 2012, **22**, 24006–24011.
126 D. Y. Kim, K. W. Choi, X. L. Zhong, Z. Y. Li, S. H. Im and O. O. Park, *CrystEngComm*, 2013, **15**, 3385–3391.
127 B. Song, D. Li, W. P. Qi, M. Elstner, C. H. Fan and H. P. Fang, *ChemPhysChem*, 2010, **11**, 585–589.
128 P. K. Jain, K. S. Lee, I. H. El-Sayed and M. A. El-Sayed, *J. Phys. Chem. B*, 2006, **110**, 7238–7248.
129 J. D. Driskell, R. J. Lipert and M. D. Porter, *J. Phys. Chem. B*, 2006, **110**, 17444–17451.
130 R. Hu, K. T. Yong, I. Roy, H. Ding, S. He and P. N. Prasad, *J. Phys. Chem. C*, 2009, **113**, 2676–2684.
131 P. Zijlstra, P. M. R. Paulo and M. Orrit, *Nat. Nanotechnol.*, 2012, **7**, 379–382.
132 H. F. Lu, H. X. Zhang, X. Yu, S. W. Zeng, K. T. Yong and H. P. Ho, *Plasmonics*, 2012, **7**, 167–173.
133 O. V. Gnedenko, Y. V. Mezentsev, A. A. Molnar, A. V. Lisitsa, A. S. Ivanov and A. I. Archakov, *Anal. Chim. Acta*, 2013, **759**, 105–109.
134 H. Zhang, D. Song, S. Gao, H. Zhang, J. Zhang and Y. Sun, *Talanta*, 2013, **115**, 857–862.
135 C.-F. Huang, G.-H. Yao, R.-P. Liang and J.-D. Qiu, *Biosens. Bioelectron.*, 2013, **50**, 305–310.
136 Y. F. Bai, F. Feng, L. Zhao, C. Y. Wang, H. Y. Wang, M. Z. Tian, J. Qin, Y. L. Duan and X. X. He, *Biosens. Bioelectron.*, 2013, **47**, 265–270.
137 R. P. Liang, G. H. Yao, L. X. Fan and J. D. Qiu, *Anal. Chim. Acta*, 2012, **737**, 22–28.
138 J. Zhang, Y. Sun, B. Xu, H. Zhang, Y. Gao, H. Q. Zhang and D. Q. Song, *Biosens. Bioelectron.*, 2013, **45**, 230–236.
139 F. Fernandez, F. Sanchez-Baeza and M. P. Marco, *Biosens. Bioelectron.*, 2012, **34**, 151–158.
140 K. Hoshino, Y. Y. Huang, N. Lane, M. Huebschman, J. W. Uhr, E. P. Frenkel and X. J. Zhang, *Lab Chip*, 2011, **11**, 3449–3457.
141 N. Pamme, *Curr. Opin. Chem. Biol.*, 2012, **16**, 436–443.
142 Y. Teramura, Y. Arima and H. Iwata, *Anal. Biochem.*, 2006, **357**, 208–215.
143 J. Pollet, F. Delport, K. P. F. Janssen, D. T. Tran, J. Wouters, T. Verbiest and J. Lammertyn, *Talanta*, 2011, **83**, 1436–1441.
144 K. V. Sreekanth, S. W. Zeng, J. Z. Shang, K. T. Yong and T. Yu, *Sci. Rep.*, 2012, **2**, 737.
145 K. V. Sreekanth, S. W. Zeng, K. T. Yong and T. Yu, *Sens. Actuators, B*, 2013, **182**, 424–428.
146 S. M. Cui, H. H. Pu, G. H. Lu, Z. H. Wen, E. C. Mattson, C. Hirschmugl, M. Gajdardziska-Josifovska, M. Weinert and J. H. Chen, *Acs Appl. Mater. Interfaces*, 2012, **4**, 4898–4904.

147 D. Jariwala, V. K. Sangwan, L. J. Lauhon, T. J. Marks and M. C. Hersam, *Chem. Soc. Rev.*, 2013, **42**, 2824–2860.
148 W. S. Hummers and R. E. Offeman, *J. Am. Chem. Soc.*, 1958, **80**, 1339.
149 E. G. Lee, K. M. Park, J. Y. Jeong, S. H. Lee, J. E. Baek, H. W. Lee, J. K. Jung and B. H. Chung, *Anal. Biochem.*, 2011, **408**, 206–211.
150 E. Hutter, J. H. Fendler and D. Roy, *J. Phys. Chem. B*, 2001, **105**, 11159–11168.
151 T. C. Peng, W. C. Lin, C. W. Chen, D. P. Tsai and H. P. Chiang, *Plasmonics*, 2011, **6**, 29–34.
152 S. Paul, D. Paul, G. R. Fern and A. K. Ray, *J. R. Soc. Interface*, 2011, **8**, 1204–1211.
153 Q. T. Liu and B. J. Boyd, *Analyst*, 2013, **138**, 391–409.
154 M. Z. Mousavi, H. Y. Chen, S. H. Wu, S. W. Peng, K. L. Lee, P. K. Wei and J. Y. Cheng, *Analyst*, 2013, **138**, 2740–2748.
155 H. X. Chen, F. Liu, K. Koh, J. Lee, Z. H. Ye, T. T. Yin and L. Z. Sun, *Microchim. Acta*, 2013, **180**, 431–436.
156 Y. Wang, J. Dostalek and W. Knoll, *Anal. Chem.*, 2011, **83**, 6202–6207.
157 H. Zhang, D. Song, S. Gao, J. Zhang, H. Zhang and Y. Sun, *Sens. Actuators, B*, 2013, **188**, 548–554.
158 L. G. Zamfir, I. Geana, S. Bourigua, L. Rotariu, C. Bala, A. Errachid and N. Jaffrezic-Renault, *Sens. Actuators, B*, 2011, **159**, 178–184.
159 C. J. Choi and S. Semancik, *Nanoscale*, 2013, **5**, 8138–8145.
160 X. S. Li, W. W. Cai, J. H. An, S. Kim, J. Nah, D. X. Yang, R. Piner, A. Velamakanni, I. Jung, E. Tutuc, S. K. Banerjee, L. Colombo and R. S. Ruoff, *Science*, 2009, **324**, 1312–1314.
161 J. Z. Shang, L. Ma, J. W. Li, W. Ai, T. Yu and G. G. Gurzadyan, *Sci. Rep.*, 2012, **2**, 792.
162 D. Han, H. Hwang and J. K. Park, *Appl. Phys. Lett.*, 2013, **102**, 054105.
163 N. Zhang, X. Yu, J. Hu, F. Xue and E. Ding, *RSC Adv.*, 2013, **3**, 13740–13747.
164 M. R. Rasch, E. Rossinyol, J. L. Hueso, B. W. Goodfellow, J. Arbiol and B. A. Korgel, *Nano Lett.*, 2010, **10**, 3733–3739.
165 H. Jang, L. Connelly, F. T. Arce, S. Ramachandran, R. Lal, B. L. Kagan and R. Nussinov, *Phys. Chem. Chem. Phys.*, 2013, **15**, 8868–8877.
166 P. A. Novick, D. H. Lopes, K. M. Branson, A. Esteras-Chopo, I. A. Graef, G. Bitan and V. S. Pande, *J. Med. Chem.*, 2012, **55**, 3002–3010.
167 Y. Kuroiwa, Y. Takakusagi, T. Kusayanagi, K. Kuramochi, T. Imai, T. Hirayama, I. Ito, M. Yoshida, K. Sakaguchi and F. Sugawara, *PLoS One*, 2013, **8**, e63073.
168 S. S. Zhao, M. A. Bichelberger, D. Y. Colin, R. Robitaille, J. N. Pelletier and J. F. Masson, *Analyst*, 2012, **137**, 4742–4750.

